Atmos. Chem. Phys., 24, 5887–5905, 2024
https://doi.org/10.5194/acp-24-5887-2024

Atmospheric Chemistry and Physics
Open Access
EGU

Measurement report: Optical characterization, seasonality, and sources of brown carbon in fine aerosols from Tianjin, North China: year-round observations

Zhichao Dong, Chandra Mouli Pavuluri, Peisen Li, Zhanjie Xu, Junjun Deng, Xueyan Zhao, Xiaomai Zhao, Pingqing Fu, and Cong-Qiang Liu

Institute of Surface-Earth System Science, School of Earth System Science, Tianjin University, Tianjin 300072, China

Correspondence: Chandra Mouli Pavuluri (cmpavuluri@tju.edu.cn)

Received: 5 May 2023 – Discussion started: 20 June 2023
Revised: 1 April 2024 – Accepted: 10 April 2024 – Published: 23 May 2024

Abstract. To investigate the optical characteristics and sources of brown carbon (BrC) in North China, where the atmospheric aerosol loadings are high and have severe impacts on Earth's climate system, we collected fine aerosols ($PM_{2.5}$) at an urban site in Tianjin over a 1-year period. We measured the ultraviolet (UV) light absorption and excitation emission matrix (EEM) fluorescence of the water-soluble BrC (WSBrC) and the water-insoluble but methanol-soluble BrC (WI-MSBrC) in the $PM_{2.5}$ using a three-dimensional fluorescence spectrometer. The average light absorption efficiency of both WSBrC ($Abs_{365,\,WSBrC}$) and WI-MSBrC ($Abs_{365,\,WI\text{-}MSBrC}$) at 365 nm was found to be highest in winter (10.4 ± 6.76 and $10.0 \pm 5.13\,Mm^{-1}$, respectively) and distinct from season to season. The averages of the fluorescence index (FI) and the biological index (BIX) of WSBrC were lower in summer than in the other seasons and opposite to that of the humification index (HIX), which implied that the secondary formation and further chemical processing of aerosols were more intensive during the summer period than in the other seasons. However, in winter, the higher HIX together with the higher FI and BIX of WI-MSBrC suggested that the BrC loading was mainly influenced by primary emissions from biomass burning and coal combustion. Based on the EEM, the types of fluorophores in WSBrC were divided into humic-like substances (HULIS), including low-oxygenated and high-oxygenated species and protein-like compounds (PLOM), though mostly PLOM in the WI-MSBrC. The direct radiation absorption by both WSBrC and WI-MSBrC in the range of 300–400 nm accounted for ~40 % of that (SFE_{Abs}, 4.97 ± 2.71 and $7.58 \pm 5.75\,W\,g^{-1}$, respectively) in the range 300–700 nm.

1 Introduction

Brown carbon (BrC) is a part of organic aerosol (OA) and can absorb solar radiation in near-ultraviolet (UV) to visible (Vis) light, ranging from 300 to 500 nm (Liu et al., 2013). It has been widely recognized that BrC has a significant effect on radiative forcing at both regional and global scales (Feng et al., 2013; Jo et al., 2016; Park et al., 2010). For example, the warming effect of water-soluble BrC in the Arctic has been reported to account for ~30 % of that exerted by the black carbon (Yue et al., 2022). The BrC not only affects the direct radiative forcing, but also has a potential impact on indirect radiative forcing due to its hydrophilicity, which influences the formation of cloud condensation nuclei (CCN) (Andreae and Gelencsér, 2006; Laskin et al., 2015). In addition, BrC is mostly composed of highly conjugated aromatic ring compounds such as a polycyclic aromatic hydrocarbons and high molecular weight substances with a polar functional group that consists of nitrogen, oxygen or humic-like substances (HULIS), which could pose a

risk to human health. For example, carbon-containing aromatic compounds can cause physical weakness, decreased immunity or arteriosclerosis, which will increase mortality due to cardiovascular and cerebrovascular diseases and a variety of cancers, such as skin cancer, pharyngeal cancer and nasal cancer (Diggs et al., 2011; Peters et al., 2008; Hecobian et al., 2010).

BrC can be emitted directly from primary sources such as biomass burning (Hoffer et al., 2006; Brown et al., 2021) and fossil-fuel combustion (Jo et al., 2016) and non-combustion processes such as bioaerosols (plant debris and fungi) and soil humus (Lin et al., 2014; Rizzo et al., 2013, 2011). On the other hand, BrC can also be produced from complex chemical reactions of volatile organic compounds (VOCs) emitted from both anthropogenic and biological origins in the gas phase and by multiphase reactions between the gaseous, particulate and aqueous constituents (Kasthuriarachchi et al., 2020; C. Li et al., 2020; Laskin et al., 2015).

In recent times, after establishing the fact that BrC absorbs light, researchers have been paying a lot of attention to measuring the physical (optical) and chemical characteristics of the BrC and estimating its climatic effects (Yue et al., 2019; Choudhary et al., 2021; Hecobian et al., 2010). However, studies on BrC are still very limited due to difficulties in the quantitative measurement of light-absorbing organic components (Corbin et al., 2019; Q. Q. Wang et al., 2022). In fact, based on the disparity in the wavelength dependence between black carbon (BC) and BrC, traditional optical instruments can be used to obtain the BrC absorption value, but the availability of such instruments is limited, which can accurately and directly differentiate the light absorption caused by the BC and BrC. On the other hand, the molecular composition and optical properties of BrC are significantly changed when the BrC is subjected to physical and photochemical processing (aging) in the atmosphere. That is why the indirect approaches have been developed to explore the molecular composition including chromophores and sources of BrC through its light absorption and fluorescence characteristics.

UV–Vis spectroscopy and excitation emission matrix (EEM) fluorescence spectroscopy are considered to be common techniques for studying the optical absorption and fluorescence chromophore optical and structural characteristics of complex organic materials, because each chromophore has its own specific excitation emission peak in the EEM maps (Q. Chen et al., 2016b; Coble, 2007). In recent years, combined spectrophotometric measurement and chemical analysis has been applied to study the BrC in Xi'an, Northwest China (Huang et al., 2018). In fact, EEM fluorescence spectroscopy provides multiple superposed spectral data. By using parallel factor (PARAFAC) analysis of such spectral data, the types of chromophores can be identified, and their types are quantified semi-quantitatively based on the range of excitation emission wavelengths (Cao et al., 2023; Zhan et al., 2022; Murphy et al., 2013). The compositions of humic-like and protein-like components have been identified from the analysis of chromophores of dissolved organic substances in aquatic environments (Xie et al., 2020). The fluorescence technique has been widely applied to measure organics in terrestrial and oceanic systems (Murphy et al., 2013; Yu et al., 2015) but has rarely been used in the study of atmospheric aerosols. Now, the application of the fluorescence technique has been well established in studying the molecular composition of aerosols as well, but studies on the identification of chromophores and thus the molecular composition of BrC in atmospheric aerosols are still very limited (Wu et al., 2021; Deng et al., 2022; Li et al., 2022; Cao et al., 2023).

Therefore, much attention needs to be paid further, particularly in long-term and continuous measurements of the optical characteristics of water-soluble BrC (WSBrC) and their temporal and spatial variations. Moreover, the investigation of light absorption and fluorescence characteristics of water-insoluble BrC (WIBrC) that can be extracted into a solvent with higher extraction efficiency is necessary to better understand the impact of the BrC on climate change (Corbin et al., 2019). In fact, such studies are very scarce, because the selection of solvents and the determination of the extraction efficiency are difficult, although different polar chromophores could be extracted by solvent extraction according to the polarity of solvents, and methanol has been used as a common solvent (Q. Chen et al., 2016a). Hence, comprehensive study of the optical properties of WSBrC and WIBrC is highly necessary to better understand the types of chromophores and optical properties of atmospheric aerosols as well as the processes of oxidation and transformations of chromophores at different locales all over the world.

China is one of the most polluted areas in the world and suffers from the absorption and scattering of solar radiation by atmospheric aerosols that directly affect the energy balance of Earth's climate system, especially in the North China Plain (D. Wang et al., 2022). As an important port city in the North China Plain, Tianjin, which has a large population, has received widespread attention in addressing atmospheric environmental issues. Previous studies have shown that BrC in the atmosphere contributes significantly to light absorption by aerosols (Deng et al., 2022). $PM_{2.5}$ loading in the Tianjin area is extremely high, with a greater abundance of organic matter (OM) (Dong et al., 2023). In such an environment, BrC is likely to become an important light-absorbing component of atmospheric aerosols. However, studies on the physicochemical characteristics and sources of BrC are very limited in the North China Plain, and to the best of our knowledge long-term observations of the optical properties and molecular composition of BrC have not been reported yet over the Tianjin region.

In this study, we measured the optical properties and molecular composition of WSBrC and water-insoluble but methanol-soluble BrC (WI-MSBrC) in fine aerosols ($PM_{2.5}$) collected from Tianjin, North China, over a 1-year period using the combined UV–Vis absorption and EEM fluorescence spectroscopy technique. We discussed the seasonal varia-

tions in the optical properties and chromophore composition of WSBrC and WI-MSBrC in the $PM_{2.5}$. We also assessed the possible sources of BrC over the Tianjin region, based on the relationships between the BrC and chemical tracers in the $PM_{2.5}$. Thus, this study provides a comprehensive understanding of the optical characteristics, seasonality and sources of BrC in the Tianjin region and warrants development of prevention and control strategies for the BrC and/or its precursor emissions.

2 Materials and methods

2.1 Aerosol sampling

Fine-aerosol ($PM_{2.5}$) sampling was conducted in Tianjin, a coastal city located at the lower reaches of the Haihe River and Bohai Sea and 150 km away from Beijing in the northern part of China. The sampling took place on the rooftop of a six-storey building at Tianjin University (ND, 39.11° N, 117.18° E) in an urban area of Nankai District, Tianjin. A high-volume air sampler (Tisch Environmental, TE-6070DX) at a flow rate of 1.0 $m^3\,min^{-1}$ and precombusted (6 h at 450 °C) quartz fiber filters (Pallflex 2500QAT-UP) were used for continuously collecting the $PM_{2.5}$ samples for 3 d (∼ 72 h) each from 5 July 2018 to 4 July 2019 ($n = 121$). Filter blanks were collected twice per season during the sample campaign, following the same sampling procedure placing the filter in a hood for 10 min without turning on the sampler pump.

Prior to and after sampling, each filter was dehumidified in a desiccator for 48 h, determined the $PM_{2.5}$ mass by gravimetric analysis, and was then stored in a precombusted glass jar with a Teflon-lined cap in the dark at −20 °C until analysis.

2.2 Measurement of carbonaceous and ionic components

Details of the measurements of aerosol organic carbon (OC), elemental carbon (EC) and water-soluble organic carbon (WSOC) were described by Wang et al. (2019) and Dong et al. (2023). Briefly, concentrations of OC and EC were measured using an aliquot of filter (1.5 cm^2) and a thermal–optical carbon analyzer (Sunset Laboratory Inc, USA), following the IMPROVE protocol of the protective visual environment. WSOC was measured using an aliquot of filter (one disk of either 14 mm or 22 mm in diameter) extracted into an organic-free Milli-Q water and total organic carbon (TOC) analyzer (Model OI, 1030W + 1088). Concentrations of K^+ and Cl^- were determined using an aliquot of filter (one disk of 22 mm in diameter) extracted into ultrapure water (> 18.2 MΩ cm) and ion chromatography (ICS-5000 System, China, Dai An) (Dong et al., 2023). The analytical uncertainty in replicate analyses was within 2 % for OC and 5 % for EC, WSOC and inorganic ions. Concentrations of all the components were corrected for field blanks.

2.3 Measurement of optical properties of BrC

2.3.1 Extraction and concentration of BrC

BrC was extracted into 30 mL ultrapure water using a sample filter disk of 22 mm in diameter placed in a glass bottle with a screw cap and sealed with Teflon tape under ultrasonication for 30 min. The extracts were filtered through a 0.45 µm polytetrafluoron (PTFE) syringe filter to remove the water-insoluble particles and filter debris and transferred into a clean glass bottle. The extracts were used for the light absorption and fluorescence measurements of WSBrC, while the concentration of WSBrC was considered the concentration of WSOC.

After the extraction of WSBrC, WI-MSBrC was extracted into 30 mL methanol using the same filter sample left in the same glass bottle with a screw cap sealed with Teflon tape under ultrasonication for 30 min. The extracts were filtered using the same 0.45 µm PTFE syringe filter to remove the insoluble particles and filter debris and transferred into another clean glass bottle. The methanol extracts were used for the measurements of optical properties of WI-MSBrC. The concentration of water-insoluble organic carbon (WIOC) was considered the concentration of WI-MSBrC, which was calculated as Eq. (1), assuming that all the water-insoluble organic contents are dissolved in methanol, although we do not preclude the possibility that some of the organic species will not be soluble in MeOH (Shetty et al., 2019).

$$\text{WI-MSBrC} = \text{OC} - \text{WSOC} \tag{1}$$

2.3.2 Light absorption of BrC

A three-dimensional fluorescence spectrometer (Aqualog, Horiba Scientific) was used to record the EEM spectra and ultraviolet–visible (UV–Vis) absorption spectra of the solution samples in 1 cm × 1 cm quartz cuvettes. The instrument parameters during sample analysis were as follows. The UV–Vis absorption spectra of extracts were recorded in the wavelength range of 240–700 nm. The UV–Vis absorption spectra of the solvents were also recorded to subtract their contributions from the extract spectra. The EEM was recorded in the wavelength range of 240–700 nm for excitation, and the integration time was 0.1 s with a 1 nm increment. An increment of 8 pixels (5.04 nm) is used as the emission wavelength interval. Prior to sample analysis, the pure solvents of water and MeOH were used to obtain the reference signal.

Based on the light absorption spectra, the absorption data are converted to the absorption coefficient (Abs: m^{-1}) following Eq. (2) (Deng et al., 2022; Hecobian et al., 2010):

$$\text{Abs}_\lambda = (A_\lambda - A_{700}) \times \frac{V_l}{V_a} \times \ln(10), \tag{2}$$

where A_{700} is the absorption at 700 nm, serving as a reference to account for baseline drift; V_l is the volume of water or MeOH used for extraction; V_a is the volume of sampled air; and L is the optical path length (0.01 m). A factor of ln(10) is utilized to convert the log base 10 to a natural logarithm to obtain a base-e absorption coefficient. To compensate for any baseline shift that may occur during analysis, absorption at wavelengths below 700 nm is compared to that of 700 nm where no absorption occurs for ambient aerosol extracts. The average absorption coefficient between 360 and 370 nm (Abs_{365}) is used to represent BrC absorption in order to avoid any interferences from non-organic compounds (e.g., nitrate) and to be consistent with the literature values (Huang et al., 2018).

The absorption Ångström exponent (AAE, Å) represents the spectral dependence of aerosol light absorption. The spectral dependence of light absorption by chromophores in solution can be described by the following Eq. (3):

$$\mathrm{Abs}_\lambda = C \times \lambda^{-\mathrm{AAE}}, \tag{3}$$

where C is a composition-dependent constant, and λ is the wavelength (nm). The AAE of the filter extracts is calculated by a formula in the wavelength range of 300–500 nm. The selected range serves two purposes: (1) to prevent any interferences from non-organic compounds at lower wavelengths and (2) to ensure a sufficient signal-to-noise ratio for the investigated samples (Huang et al., 2018).

The mass absorption efficiency (MAE: $m^2\,g^{-1}$) of the filter extract at a wavelength of λ can be characterized as Eq. (4). The ratio of MAE_{250} to MAE_{365} is denoted as E_2/E_3 to characterize the relative size of the molecular weight, which is inversely proportional to the molecular weight. E_2/E_3 is calculated with the method as Eq. (5).

$$\mathrm{MAE}_\lambda = \mathrm{Abs}_\lambda / M \tag{4}$$

$$\frac{E_2}{E_3} = \frac{\mathrm{MAE}_{250}}{\mathrm{MAE}_{365}} \tag{5}$$

M ($\mu g\,m^{-3}$) is the concentration of WSOC for water extracts and that of WIOC for methanol extracts.

The imaginary part (k) of the refractive index ($m = n + ik$) is derived with the following Eq. (6) (Liu et al., 2013; Deng et al., 2022):

$$k_\lambda = (\mathrm{MAE} \times \rho \times \lambda)/4\pi, \tag{6}$$

where MAE is the mass-absorption cross section of WS-BrC or WI-MSBrC ($m^2\,g^{-1}$), ρ is the effective density, and λ is the wavelength for the computed MAE including WS-BrC and WI-MSBrC. For this study, an effective density of 1.5 $g\,m^{-3}$ is assumed for WSBrC and WI-MSBrC in the derivation (Liu et al., 2013). MAE values are computed for 365 nm.

2.3.3 EEM of BrC and PARAFAC analysis

The raw EEMs were first calibrated for the correction of spectrometer factors, which reflect the spectrometer deviation and light source, and then for the inner filter correction, following the procedure described elsewhere (Chen et al., 2019; Gu and Kenny, 2009). Briefly, the inner filter correction of the EEMs was done based on the UV–Vis light absorbance of the extracts, which was lower than 0.7 in the calibrated wavelength range and is appropriate (Gu and Kenny, 2009). The signal intensity of the EEMs was then normalized to the Raman unit (RU) of water (Lawaetz and Stedmon, 2009). The fluorescence volume (FV, RU-nm^2) of extracts present in the atmosphere was estimated based on the EEMs at the excitation wavelength ranging from 240 to 700 nm and then normalized it (i.e., normalized fluorescence volume, NFV; RU-nm^2 $(mg\,L^{-1})^{-1}$) by dividing the FV by the concentration of WSOC and WIOC in the aerosol ($mg\,m^{-3}$).

Various types of chromophores present in the $PM_{2.5}$ samples were classified and identified based on the PARAFAC analysis of the EEMs using the SOLO (Eigenvector Inc.) data analysis software. PARAFAC analysis was performed for each extraction fluid in each season. Ultimately, three EEM components were determined and assigned to different types of chromophores.

Additionally, the fluorescence index (FI) was determined by calculating the ratio of emission intensities at 450 and 500 nm after excitation at 370 nm (McKnight et al., 2001). Contributions from local biological sources can be characterized by the biological index (BIX), which was calculated using the ratio of emission intensities at 380 and 430 nm following 310 nm excitation (Gao and Zhang, 2018). Under the condition of Ex = 255 nm, the humification index (HIX) was determined by dividing the area of the fluorescence intensity between 435 and 480 nm by that of the fluorescence intensity between 300 and 345 nm (Battin, 1998). The calculation formulas (Eqs. 7–9) are as follows.

$$\mathrm{FI} = \frac{F_{450}}{F_{500}},\ \lambda_{\mathrm{Ex}} = 370\,\mathrm{nm} \tag{7}$$

$$\mathrm{BIX} = \frac{F_{380}}{F_{430}},\ \lambda_{\mathrm{Ex}} = 310\,\mathrm{nm} \tag{8}$$

$$\mathrm{HIX} = \frac{\int 435\text{–}480}{\int 300\text{–}345},\ \lambda_{\mathrm{Ex}} = 255\,\mathrm{nm} \tag{9}$$

In Eqs. (6)–(8), λ_{Ex} refers to the excitation wavelength, F_i refers to the fluorescence intensity of the emission wavelength at i in the emission spectrum, and $\int i\text{–}j$ refers to the integrated fluorescence emission intensity in the range of 435–480 to 300–345 nm.

2.3.4 Simple forcing efficiency by light absorption of BrC (SFE_{Abs})

It is possible to make a rough estimate of the radiative forcing caused by aerosols using an SFE ($W\,g^{-1}$), which reflects the energy added to Earth's atmospheric system per unit mass of aerosols and can be estimated as described in the literature (Bond and Bergstrom, 2006; Deng et al., 2022), using the following Eq. (10):

$$\frac{\mathrm{dSFE}}{\mathrm{d}\lambda} = -\frac{1}{4}\frac{\mathrm{d}S(\lambda)}{\mathrm{d}\lambda}\tau_{\mathrm{atm}}^{2}(\lambda)(1-F_{\mathrm{c}}) \times \left[2(1-a_{\mathrm{s}})^{2}\beta(\lambda)\times \mathrm{MSE}(\lambda) - 4a_{\mathrm{s}}\times \mathrm{MAE}(\lambda)\right], \quad (10)$$

where $\mathrm{d}S/\mathrm{d}\lambda$ is the solar irradiance, τ_{atm} is the atmospheric transmission (0.79), F_{c} is the cloud fraction (approximately 0.6), a is the surface albedo (average 0.19), β is the backscatter fraction, and MSE and MAE are the mass scattering and absorption efficiency, respectively (Deng et al., 2022).

It is important to note that BrC can affect a strong instantaneous negative forcing through scattering. However, it is not possible to evaluate this directly using offline samples because of strong dependency on particle size. That is why we were limited to estimating the radiative effect caused by only the absorption component of the BrC in this study. Therefore, Eq. (10) can be simplified to

$$\mathrm{SFE}_{\mathrm{Abs}} = \int \frac{\mathrm{d}S(\lambda)}{\mathrm{d}\lambda}\tau_{\mathrm{atm}}^{2}(1-F_{\mathrm{c}})a_{\mathrm{s}}\mathrm{MAE}(\lambda)\mathrm{d}\lambda. \quad (11)$$

3 Results and discussion

3.1 Characteristics of ultraviolet light absorption of WSBrC and WI-MSBrC

3.1.1 Absorption coefficient

Annual and seasonal averages of various optical properties of the WSBrC and WI-MSBrC in $PM_{2.5}$ measured in this study are summarized in Table 1. Their ranges and median values are provided in Table S1 in the Supplement. Temporal variations in the absorption coefficient of WSBrC at 365 nm ($Abs_{365(WSBrC)}$) and that of WI-MSBrC ($Abs_{365(WI\text{-}MSBrC)}$) together with the concentrations of WSOC and WIOC are depicted in Fig. 1. Because the light absorption at the wavelength of 365 nm would not be interfered with by inorganic substances (Hecobian et al., 2010), the Abs at 365 nm was selected for the analysis in this study. $Abs_{365(WSBrC)}$ ranged from 0.49 to 36.7 Mm^{-1} with an average of 4.74 Mm^{-1} during the campaign, while $Abs_{365(WI\text{-}MSBrC)}$ ranged from 0.32 to 25.0 Mm^{-1} (avg 3.87 Mm^{-1}) during the campaign. Temporal trends of $Abs_{365(WSBrC)}$ were found to be similar to those of $Abs_{365(WI\text{-}MSBrC)}$, with the lowest levels in summer followed by a gradual increase toward fall and a peak in winter and then a gradual decrease toward spring during the campaign (Fig. 1). Furthermore, those trends were highly comparable to those of the concentrations of both WSOC and WIOC in $PM_{2.5}$ (Fig. 1). The correlations between $Abs_{365(WSBrC)}$ and WSOC and between $Abs_{365(WI\text{-}MSBrC)}$ and WIOC were found to be strong ($R = 0.93$ and 0.96, respectively) during the campaign. These results indicate that both WSBrC and WI-MSBrC might have been derived from the same or similar sources including the secondary processes, and their light absorbance should have been significantly dependent on their abundances that varied from season to season (Fig. 1; Table 1).

Averages of both $Abs_{365(WSBrC)}$ and $Abs_{365(WI\text{-}MSBrC)}$ were highest in winter, followed by fall and spring, and lowest in summer (Table 1). The high Abs_{365} of BrC in winter might have been mainly driven by the existence of large amounts of organic aerosols, whereas the lowest Abs_{365} in summer might be due to enhanced decomposition of BrC constituents by photobleaching under high solar radiation and oxidant loading in the atmosphere, which is unlikely in winter. The seasonal variations of both $Abs_{365(WSBrC)}$ and $Abs_{365(WI\text{-}MSBrC)}$ in Tianjin were similar to those of the Abs_{365} of WSBrC reported in the southeastern United States, but their values (Table 1) were much higher than that (0.3–3.0 Mm^{-1} in 2007) in the southeastern United States (Hecobian et al., 2010) as well as those in Atlanta and Los Angeles (0.88 ± 0.71 and 0.61 ± 0.38 Mm^{-1}, respectively) in the summer of 2010 (Zhang et al., 2011). Biomass burning was considered to be the dominant source of BrC in the southeastern United States in colder periods, whereas both primary emissions from fossil-fuel combustion and secondary formation were significant in summer (Hecobian et al., 2010), while the secondary organic aerosol (SOA) formed from fresh anthropogenic and biogenic VOCs was considered to be significant in Atlanta and Los Angeles, respectively (Zhang et al., 2011).

It has been reported that the solid-fuel (i.e., biomass or coal) combustion is dominant, and the Abs_{370} of BrC is reported to be high (21.8 Mm^{-1}) in North Chinese cities (Zhang et al., 2021). It has also been reported that the Abs_{370} of BrC produced by residential wood burning is much higher, reaching up to 37.1 ± 74.6 Mm^{-1} in Athens in winter (Liakakou et al., 2020). The maximum $Abs_{365(WSBrC)}$ and $Abs_{365(WI\text{-}MSBrC)}$ in Tianjin aerosols were 36.7 and 25.0 Mm^{-1}, respectively, which are comparable to those of wood combustion samples. However, their ranges were found to be large during the campaign (Fig. 1; Table S1), suggesting that, in addition to biomass burning, the other emission sources and meteorological conditions in different seasons should have played an important role in controlling the WSBrC and WI-MSBrC loadings and their optical characteristics in the Tianjin atmosphere. Furthermore, the $Abs_{365(WSBrC)}$ observed in this study (Table 1) is slightly lower compared to that reported in Tianjin during the winter of 2016 (14.1 ± 8.5 Mm^{-1}) and the summer of 2017 (2.1 ± 1.0 Mm^{-1}) (Deng et al., 2022) as well as those reported in Beijing and Xi'an, which are considered to be highly polluted cities in North China (Huang et al.,

Table 1. Mass concentrations of the WSOC, WIOC and absorbance efficiency of WSBrC and WI-MSBrC (avg ± SD) in $PM_{2.5}$ from Tianjin, North China.

		Annual	Summer	Fall	Winter	Spring
Concentrations						
WSOC ($\mu g\,m^{-3}$)		3.25 ± 2.18	1.88 ± 0.53	3.45 ± 1.71	5.06 ± 2.99	2.48 ± 0.82
WIOC ($\mu g\,m^{-3}$)		1.68 ± 1.77	0.43 ± 0.32	1.55 ± 1.04	3.74 ± 2.09	0.88 ± 0.63
Optical parameters						
WSBrC	Abs_{365} (Mm^{-1})	4.74 ± 5.10	1.47 ± 0.77	3.71 ± 2.83	10.4 ± 6.76	3.45 ± 2.29
	MAE_{365} ($m^2\,g^{-1}$)	1.28 ± 0.66	0.80 ± 0.44	0.96 ± 0.33	2.04 ± 0.46	1.31 ± 0.55
	AAE (300–500 nm)	5.66 ± 0.82	5.17 ± 0.83	6.21 ± 0.65	5.88 ± 0.58	5.42 ± 0.74
	E_2/E_3	5.36 ± 0.91	5.64 ± 1.21	5.78 ± 0.83	5.19 ± 0.44	4.83 ± 0.64
	FI	1.38 ± 0.09	1.31 ± 0.07	1.47 ± 0.07	1.37 ± 0.02	1.37 ± 0.09
	BIX	1.05 ± 0.13	0.91 ± 0.06	1.06 ± 0.08	1.20 ± 0.08	1.01 ± 0.11
	HIX	2.87 ± 0.53	3.12 ± 0.44	3.11 ± 0.51	2.47 ± 0.43	2.76 ± 0.47
	k_{365}	0.056 ± 0.029	0.035 ± 0.020	0.042 ± 0.015	0.089 ± 0.021	0.057 ± 0.024
	$SFE_{Abs300—400}$ ($W\,g^{-1}$)	1.95 ± 1.02	1.21 ± 0.67	1.99 ± 0.84	3.12 ± 0.71	1.46 ± 0.52
	$SFE_{Abs300—700}$ ($W\,g^{-1}$)	4.97 ± 2.71	3.68 ± 2.58	5.12 ± 2.17	7.60 ± 2.17	3.39 ± 1.42
WI-MSBrC	Abs_{365} (Mm^{-1})	3.87 ± 4.69	0.74 ± 0.25	2.83 ± 2.51	10.0 ± 5.13	1.99 ± 1.95
	MAE_{365} ($m^2\,g^{-1}$)	2.36 ± 1.26	2.50 ± 1.78	1.86 ± 1.02	2.69 ± 0.36	2.41 ± 1.28
	AAE (300–500 nm)	6.06 ± 1.23	5.49 ± 1.26	6.11 ± 1.86	6.30 ± 0.27	6.27 ± 0.90
	E_2/E_3	6.60 ± 2.04	6.79 ± 1.32	5.77 ± 1.35	6.20 ± 0.44	7.60 ± 3.25
	FI	1.60 ± 0.13	1.58 ± 0.12	1.57 ± 0.06	1.73 ± 0.11	1.51 ± 0.11
	BIX	1.26 ± 0.21	1.32 ± 0.18	1.05 ± 0.14	1.43 ± 0.09	1.23 ± 0.18
	HIX	0.81 ± 0.60	0.25 ± 0.08	1.23 ± 0.61	1.33 ± 0.30	0.42 ± 0.28
	k_{365}	0.104 ± 0.057	0.109 ± 0.079	0.081 ± 0.045	0.117 ± 0.016	0.105 ± 0.057
	$SFE_{Abs300—400}$ ($W\,g^{-1}$)	2.98 ± 1.70	1.21 ± 0.67	2.98 ± 1.52	4.13 ± 0.57	3.61 ± 1.91
	$SFE_{Abs300—700}$ ($W\,g^{-1}$)	7.58 ± 5.75	3.68 ± 2.58	8.69 ± 9.23	9.36 ± 4.51	8.70 ± 5.03

2020; J. Li et al., 2020). However, the $Abs_{365(WSBrC)}$ and $Abs_{365(WI\text{-}MSBrC)}$ found in winter in this study were higher than those reported at different locations in South China – Nanjing ($Abs_{365(WSBrC)} = 4.84\,Mm^{-1}$, $Abs_{365(MSBrC)} = 7.75\,Mm^{-1}$) (Xie et al., 2020), Guangzhou ($Abs_{365(WSBrC)} = 8.8\,Mm^{-1}$) (Li et al., 2018) and Lhasa ($Abs_{365(WSBrC)} = 1.04\,Mm^{-1}$, $Abs_{365(MSBrC)} = 1.47\,Mm^{-1}$) (Zhu et al., 2018) – where the fossil-fuel combustion is considered the dominant source. Such higher Abs_{365}, particularly in winter, indicates that BrC in $PM_{2.5}$ in Tianjin might have been derived from mixed sources such as biomass burning and fossil-fuel (coal) combustion and have a significant effect on light absorption and thus on the climate system over the region.

Figure 2 shows the seasonal average absorption spectra of WSBrC and WI-MSBrC at wavelengths of 240–700 nm, which show the common feature that the absorption of shorter wavelengths increases sharply and significantly. Such a feature is different from the absorption characteristics of BC, whose AAE is close to 1 and weakly dependent on the wavelength. Another evident feature of BrC absorption spectra shown in Fig. 2 is that the Abs of WI-MSBrC was always greater than that of WSBrC across the shorter wavelengths in winter and in the range of 260–300 nm in the other seasons, which is consistent with the pattern reported in the literature (Huang et al., 2020; J. Li et al., 2020). In addition, the Abs of WI-MSBrC peaked at 280 nm, but not that of WSBrC (Fig. 2). Such patterns can be attributed to the difference in types and amounts of chromophores soluble in water and methanol (e.g., PAHs are soluble in methanol, but not in water). It is noteworthy that π–π^* electron transitions in the double bonds of aromatic compounds are the primary cause of light absorption in the wavelength range of 250–300 nm. It has been reported in another study that nitroaromatics have contributed 60 % to the total absorbance in the 300–400 nm range (Hems et al., 2021). The electron transitions in phenolic arenes, aniline derivatives, polyenes and polycyclic aromatic hydrocarbons with two or more rings are responsible for the absorbance in the bands between 270 and 280 nm (Baduel et al., 2009). Therefore, the differences observed in the Abs of WSBrC and WI-MSBrC imply that the aromatic and/or unsaturated aliphatic organic compounds are abundant in $PM_{2.5}$ in Tianjin and are more soluble in MeOH than in water.

High correlations ($R = 0.73$–0.97) were found between the Abs_{365} of both WSBrC and WI-MSBrC and WSOC and WIOC in each season, except in summer ($R = 0.20$–0.62)

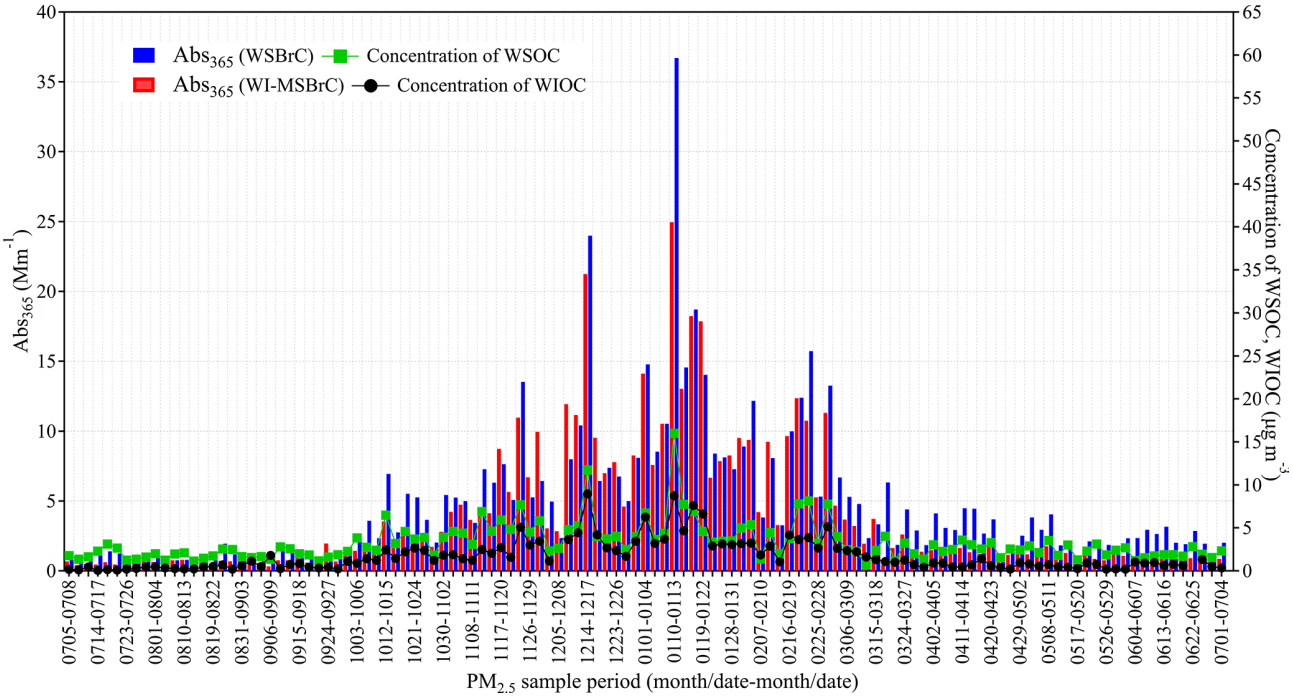

Figure 1. Temporal variations of the light absorption coefficient of water-soluble brown carbon (BrC) at 365 nm ($Abs_{365(WSBrC)}$), water-insoluble but methanol-soluble BrC ($Abs_{365(WI\text{-}MSBrC)}$) and the mass concentrations of WSOC and WIOC in $PM_{2.5}$ in Tianjin, North China, during 2018 and 2019. WSOC and WIOC mass concentration data were obtained from Dong et al. (2023).

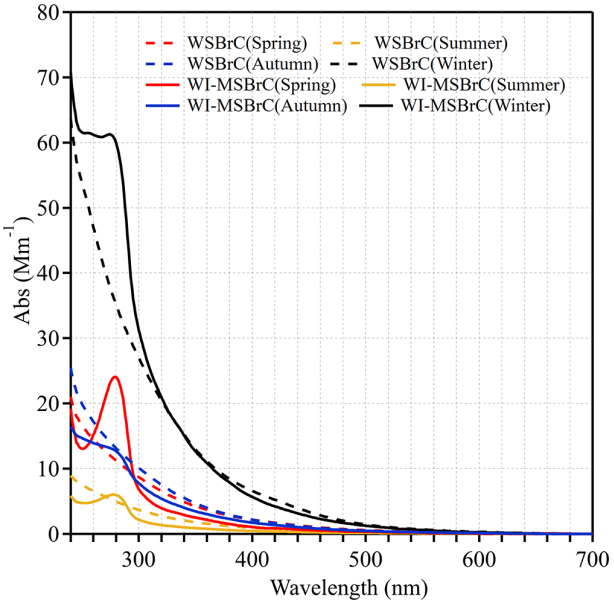

Figure 2. Seasonal averages of absorption spectra in the wavelength range of 240–700 nm of WSBrC and WI-MSBrC in $PM_{2.5}$ from Tianjin, North China.

(Fig. S1 in the Supplement). As noted earlier, such linearity of Abs_{365} with WSOC and WIOC indicates that WSBrC and WI-MSBrC might have been derived from similar sources, including the secondary processes over the Tianjin region, except in summer, because the light absorption efficiency of organic compounds of different origins are different and significantly depend on their secondary processes in the atmosphere (Zhong and Jang, 2011). In fact, the Abs depends on the amount of BrC availability but not on the total OC content. In summer, the BrC loading might be less due to either photobleaching under the enhanced aging and/or less availability of N and/or S species to produce N- and S-containing organics (BrC) in the atmosphere over the Tianjin region.

The moderate to high positive correlations ($R = 0.51$–0.92) found between both $Abs_{365(WSBrC)}$ and $Abs_{365(WI\text{-}MSBrC)}$ and K^+ and Cl^- in all seasons, except between $Abs_{365\,WSBrC}$ and Cl^- in summer ($R = 0.29$) (Fig. S2 in the Supplement), suggest that biomass burning and coal combustion were major sources (Dong et al., 2023) of BrC in the Tianjin region. The poor correlation between Abs_{365} and K^+ was driven by two outliers obtained in K^+ data that might have occurred due to unknown biomass burning events at the local scale. In addition, the correlation between $Abs_{365(WSBrC)}$ and K^+ was relatively stronger than that between $Abs_{365(WI\text{-}MSBrC)}$ and K^+, except in summer (Fig. S2), which supports the chromophores, like nitrophenols, derived from biomass burning being potentially more water-soluble (J. Li et al., 2020). The correlation between $Abs_{365(WI\text{-}MSBrC)}$ and Cl^- was relatively stronger than that between $Abs_{365(WSBrC)}$ and Cl^- in spring and summer and

comparable in fall, which suggests that the chromophores derived from fossil-fuel (e.g., coal) combustion are slightly more soluble in MeOH compared to that in water and were abundant in spring and summer in Tianjin.

3.1.2 AAE

The magnitude of the AAE can reflect the sources and atmospheric chemical processes of BrC (Lack et al., 2013), because the AAE of the BrC emitted from fossil-fuel combustion was found to be ~ 1, that from biomass burning ranged from 1 to 3 and that derived by secondary formation or transformations varied from 3 to 7 (Yan et al., 2018). It has also been reported that the AAE of light-absorbing organic species (i.e., BrC) is much larger than that of soot (BC). The AAE was found to be between 2 and 4 for the particles containing both soot and BrC. Furthermore, the AAE value of particulate matter is closely related to its chemical composition, mixing state, particle size and other factors. For example, Sun et al. (2017) reported that the average AAE of coal briquettes is 2.55 ± 0.44, whereas that of the coal chunks is 1.30 ± 0.32 (Sun et al., 2017). However, it is important to note that, unlike the direct measurement of the AAE of the particulate matter, the light absorption characteristics of organic components extracted into solvent are not affected by the particle size and mixing state of aerosols but depend on their composition. The AAE of HULIS isolated from biomass burning aerosols by water extraction followed by the separation with the exchange column was reported to be 6–7 (Hoffer et al., 2006).

The AAE of WSBrC in $PM_{2.5}$ from Tianjin ranged from 3.85 to 7.99 with an average of 5.66 during the campaign. The seasonal averages were highly comparable with each other, except for a slightly higher level in fall (Table 1). The average AAE of WSBrC in Tianjin (Table 1) is comparable to that (5.1 ± 2.0) reported from New Delhi, India, and Beijing (5.3 ± 0.4 in winter and 5.8 ± 0.5 in summer) and the outflow region (6.4 ± 0.6) of North China (Lesworth et al., 2010). The AAE of WSBrC in Tianjin was also similar to that (range 6–8) reported in the particulate matter in the southeastern United States (Hecobian et al., 2010) and downtown Atlanta (Liu et al., 2013), where both biogenic and fossil-fuel combustion emissions and secondary processes are considered significant sources. Such higher levels and comparisons of the AAE of WSBrC imply that the OA in Tianjin should have been derived from mixed sources and been substantially polar, because the AAE of BrC increases with its increasing polarity (Q. Chen et al., 2016a).

However, the AAE of WI-MSBrC in Tianjin ranged from 2.08 to 12.9 (avg 6.06) and was comparable with that of WSBrC. Furthermore, the averages of the AAE of WI-MSBrC in each season were comparable with the others, except for a relatively lower level in summer, and also with those of the AAE of WSBrC (Table 1). Generally, the water-insoluble portion is expected to have a stronger absorption and weaker wavelength dependence (Saleh, 2020). It has also been reported that the AAE values of the water extract are greater than those of the acetone and methanol extracts (Shetty et al., 2019) and interpreted that the extraction efficiency of polycyclic aromatic hydrocarbons from methanol or other organic solvents is higher than that from water, leading to a higher absorption at longer wavelengths in the methanol extract and therefore a lower AAE value. However, it has also been found that the value of $AAE_{300\text{-}600}$ of the water extract of biomass burning samples is lower than that extracted into acetonitrile (Lin et al., 2017), indicating that the origin of BrC also plays an important role. Such comparability between the AAE of WSBrC and WI-MSBrC is consistent with the pattern reported in urban Beijing during winter and Xi'an, China (J. Li et al., 2020), where the emissions from fossil-fuel combustion are dominant. These results and their comparisons again support the BrC possibly having been significantly derived from mixed sources (biomass burning and fossil-fuel combustion).

3.1.3 MAE and k

MAE provides the light-absorbing ability of BrC. The MAE_{365} of WSBrC ($MAE_{365(WSBrC)}$) ranged from $0.38\,m^2\,g^{-1}$ to 3.41 (avg $1.28\,m^2\,g^{-1}$) and lower by 2 times than that (range 0.18–$7.05\,m^2\,g^{-1}$; avg $2.36\,m^2\,g^{-1}$) of WI-MSBrC ($MAE_{365(WI\text{-}MSBrC)}$) during the campaign in Tianjin. Although the seasonal averages of both $MAE_{365(WSBrC)}$ and $MAE_{365(WI\text{-}MSBrC)}$ were higher in winter (1.28 and $2.36\,m^2\,g^{-1}$, respectively), the former showed the second highest value in spring followed by fall and the lowest value in summer, whereas the latter showed the second highest value in summer followed by spring and the lowest value in fall (Table 1). Furthermore, the average $MAE_{365(WSBrC)}$ in winter was 2.5 times higher than that in summer, which is similar to that (1.8 times) reported earlier in Tianjin (Deng et al., 2022), whereas the difference between the averages of $MAE_{365(WI\text{-}MSBrC}$ in winter to fall is 1.4 times only. The seasonal variations of $MAE_{365(WSBrC)}$ and $MAE_{365(WI\text{-}MSBrC)}$ found in this study are similar to those reported in Xi'an (J. Li et al., 2020).

The imaginary refractive index (k) is another important parameter that represents the light-absorbing ability of carbon and that is applied in the climate model to assess the direct radiative forcing of aerosols. The k of WSBrC ($k_{365(WSBrC)}$) and WI-MSBrC ($k_{365(WI\text{-}MSBrC)}$) in Tianjin ranged from 0.017 to 0.149 and from 0.008 to 0.307, respectively, in Tianjin. Interestingly, the average $k_{365(WI\text{-}MSBrC)}$ was 1.9 times that of $k_{365(WSBrC)}$ during the campaign (Table 1), and their seasonal patterns were also similar to those of the $MAE_{365(WSBrC)}$ and $MAE_{365(WI\text{-}MSBrC)}$ (Table 1).

Both these MAE_{365} and k_{365} results indicate that most of the light-absorbing chromophores are insoluble in water but soluble in MeOH, and their abundances are significantly variable from season to season. Such large seasonal differences

indicate that the BrC sources and formation and/or transformation including the degradation (photobleaching) processes might be different in each season. The higher levels of MAE_{365} and k_{365} in winter suggest that the contributions of OA from coal combustion and biomass burning emissions were significantly higher than those in the other seasons due to increased residential heating activities. The lower $MAE_{365(WSBrC)}$ and $k_{365(WSBrC)}$ and the second highest values of $MAE_{365(WI\text{-}MSBrC)}$ and $k_{365(WI\text{-}MSBrC)}$ in summer imply that the contributions of OA from fossil-fuel combustion emissions might be dominant, and the subsequent photobleaching of WSBrC might be significant under high solar radiation in summer.

The ratio of MAE_{250} to MAE_{365}, which is inversely correlated with the molecular size and aromaticity (Q. C. Chen et al., 2016) of WSBrC ($E_2/E_{3(WSBrC)}$) and WI-MSBrC ($E_2/E_{3(WI\text{-}MSBrC)}$) in Tianjin, ranged from 3.30 to 6.25 with averages of 4.83 and 4.50–24.1 (avg 7.61), respectively, during the campaign. Interestingly, the averages of $E_2/E_{3(WSBrC)}$ were comparable in summer and fall and higher than those in winter and spring (Table 1), whereas the average $E_2/E_{3(WI\text{-}MSBrC)}$ was higher in spring, followed by summer and winter, and lowest in fall and higher than the $E_2/E_{3(WSBrC)}$ in each season, except in fall. Both $E_2/E_{3(WSBrC)}$ and $E_2/E_{3(WI\text{-}MSBrC)}$ in each season were comparable or relatively higher than the E_2/E_3 of HULIS (4.7 ± 0.27 for herbaceous plants, 3.6 ± 0.18 for shrubs, 4.2 ± 0.77 for evergreen trees, 4.0 ± 0.82 for deciduous trees, 5.8 ± 0.5 for rice straw, 4.5 ± 0.2 for corn straw and 4.4 ± 0.3 for pine branches) emitted from biomass burning (Tang et al., 2020) and lower than that (14.7 ± 0.7) of HULIS emitted from coal combustion (Fan et al., 2016). Thus, $E_2/E_{3(WSBrC)}$ and $E_2/E_{3(WI\text{-}MSBrC)}$ and their comparisons with source signatures indicate that both WSBrC and WI-MSBrC in $PM_{2.5}$ over the Tianjin region should have been mainly derived from biomass burning, followed by coal combustion and consisting of high aromaticity and large molecular sizes.

3.2 Direct radiative forcing of WSBrC and WI-MSBrC

Radiative forcing efficiencies of WSBrC and WI-MSBrC were calculated by integrating the wavelength-dependent SFE_{Abs} from 300 to 700 nm ($SFE_{Abs300–700(WSBrC)}$ and $SFE_{Abs300–700(WI\text{-}MSBrC)}$, respectively) in this study. $SFE_{Abs300–400}$ was also integrated to estimate the radiative forcing efficiencies of WSBrC ($SFE_{Abs300–400(WSBrC)}$) and WI-MSBrC ($SFE_{Abs300–400(WI\text{-}MSBrC)}$), because the BrC strongly absorbs light in the UV–Vis range. The temporal variations of SFE_{Abs} of WSBrC and WI-MSBrC in both wavelength ranges are shown in Fig. 3. $SFE_{Abs300–700(WSBrC)}$ and $SFE_{Abs300–400(WSBrC)}$ ranged from 0.98 to 13.1 $W\,g^{-1}$ with averages of 4.97 $W\,g^{-1}$ and 0.60–5.13 $W\,g^{-1}$ (avg 1.95 $W\,g^{-1}$), respectively, whereas $SFE_{Abs300–700(WI\text{-}MSBrC)}$ and $SFE_{Abs300–400(WI\text{-}MSBrC)}$ were 0.92–51.3 $W\,g^{-1}$ (7.58 $W\,g^{-1}$) and 0.64–8.84 $W\,g^{-1}$ (2.98 $W\,g^{-1}$), respectively, and were higher by 1.5 times that of $SFE_{Abs300–700(WSBrC)}$ and $SFE_{Abs300–400(WSBrC)}$ (Table 1). Further, both the integrated average $SFE_{Abs300–700(WSBrC)}$ and $SFE_{Abs300–700(WI\text{-}MSBrC)}$ were higher by 2.5 times that of $SFE_{Abs300–400(WSBrC)}$ and $SFE_{Abs300–400(WI\text{-}MSBrC)}$ (Table 1). Temporal variations of both $SFE_{Abs300–400(WSBrC)}$ and $SFE_{Abs300–700(WSBrC)}$ were found to be quite similar, with a clear seasonal pattern with the lowest levels in summer followed by a gradual increase toward fall to a peak in winter and then a gradual decrease toward spring to the lowest levels in summer, except for a sharp rise in early summer 2019 (Fig. 3). $SFE_{Abs300–400(WI\text{-}MSBrC)}$ and $SFE_{Abs300–700(WI\text{-}MSBrC)}$ showed exactly the same temporal pattern albeit different from that of $SFE_{Abs300–400(WSBrC)}$ and $SFE_{Abs300–700(WSBrC)}$ (Fig. 3). The levels of $SFE_{Abs300–400(WI\text{-}MSBrC)}$ and $SFE_{Abs300–700(WI\text{-}MSBrC)}$ were found to be relatively stable throughout each season, except in spring, with higher levels in spring followed by winter and lower levels in summer (Fig. 3). Consistent with these seasonal patterns, the seasonal variations of $k_{365(WSBrC)}$ and $k_{365(WI\text{-}MSBrC)}$, vital parameters that reflect the light-absorbing ability and that are used in the estimation of radiative forcing by the climate model (Shamjad et al., 2016), also showed a similar pattern (Fig. S3 in the Supplement).

The SFE_{Abs} of both WSBrC and WI-MSBrC in both the spectral ranges was higher in winter (Table 1). However, $SFE_{Abs300–400(WSBrC)}$ and $SFE_{Abs300–700(WSBrC)}$ showed the second highest values in fall and the lowest and comparable values in summer and spring (Table 1), whereas $SFE_{Abs300–400(WI\text{-}MSBrC)}$ and $SFE_{Abs300–700(WI\text{-}MSBrC)}$ showed the second highest and comparable values in spring and fall and the lowest values in summer (Table 1). It is noteworthy that $SFE_{Abs300–400(WSBrC)}$, $SFE_{Abs300–700(WSBrC)}$, $SFE_{Abs300–400(WI\text{-}MSBrC)}$ and $SFE_{Abs300–700(WSBrC)}$ were higher by 61 %, 52 %, 71 % and 61 %, respectively, in winter than those in summer, indicating that the abundance and strong light absorption capacity of BrC in winter led to a significant increase in direct radiative forcing by BrC. Furthermore, $SFE_{Abs300–400}$ accounted for 40 % of $SFE_{Abs300–700}$ in both fractions of BrC during the whole campaign period, and their seasonal averages varied between 33 % and 44 %, which are similar to those reported in Tianjin by Deng et al. (2022), indicating that the light absorption by BrC in the UV–Vis range plays a significant role in the total BrC radiative forcing.

Furthermore, it is important to note that it has been reported that the direct radiative effect of WSBrC is 12.5 % and 13.5 % relative to BC radiative forcing in the 280–4000 nm range in summer and winter, respectively, in Tianjin (Deng et al., 2022). In fact, as noted above, the annual average $SFE_{Abs300–700(WI\text{-}MSBrC)}$ is higher by 1.5 times that of $SFE_{Abs300–700(WSBrC)}$ (Table 1) in Tianjin. Therefore, the direct radiative effect of the total ($\sum$WSBrC + WI-MSBrC) BrC relative to BC would become $\sim$ 32.5 % in Tianjin, re-

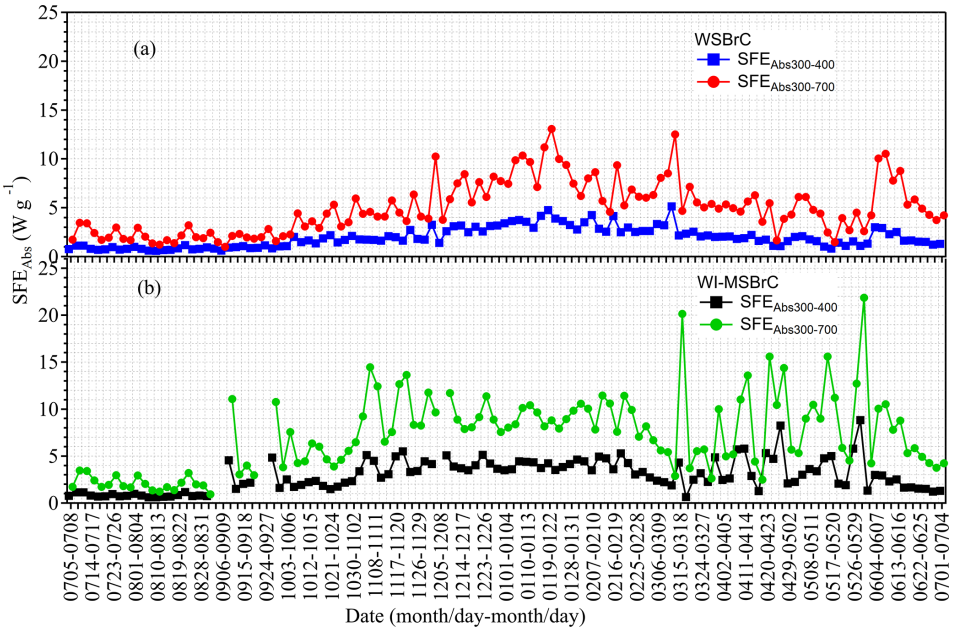

Figure 3. Temporal variations in the SFE_{Abs} of WSBrC and WI-MSBrC from 300–400 and 300–700 nm in $PM_{2.5}$ from Tianjin.

vealing that the BrC plays a greater role in light-absorbing aerosols in the shorter-wavelength region in comparison to the entire spectrum.

3.3 Fluorescence characteristics of WSBrC and WI-MSBrC

3.3.1 Fluorescence indices

Annual and seasonal averages of the fluorescence indices FI, BIX and HIX of WSBrC (FI_{WSBrC}, BIX_{WSBrC} and HIX_{WSBrC}, respectively) and WI-MSBrC ($FI_{WI\text{-}MSBrC}$, $BIX_{WI\text{-}MSBrC}$ and $HIX_{WI\text{-}MSBrC}$, respectively) in $PM_{2.5}$ at Tianjin are presented in Table 1. Their ranges and median values are provided in Table S1, and the temporal variations are depicted in Fig. 3. Fluorescence indices are developed as indicators for the type and source of the fluorescent OM in aquatic and soil systems and have been successfully applied to assess the sources and aging processes of OA in the atmosphere in recent times (Dong et al., 2023; Lee et al., 2013; Wu et al., 2021). FI and BIX provide insights into exploring the source and aging of OA and have received much attention in recent times (Xie et al., 2020; Gao and Zhang, 2018; Qin et al., 2018; Deng et al., 2022). They have been considered as indicators to assess the relative contributions of terrestrial, biological and microbially derived OM to OA. FI values of OM lower than 1.4 indicate its terrestrial origin, and values of 1.9 or higher indicate microbial origin and show an inverse relationship with the aromaticity of the OM (Gao and Zhang, 2018; Birdwell and Engel, 2010). The BIX values of 0.8 and 1.0 correspond to the freshly derived OM of biological or microbial origin, and those of $\sim$0.6 imply little contribution of the biological OM (Birdwell and Engel, 2010; Dong et al., 2023). HIX reflects the degree of humification of OA and has been considered a proxy for aromaticity of OM, and the HIX value increases with the increasing aromaticity and polycondensation degree (Deng et al., 2022; McKnight et al., 2001; Birdwell and Engel, 2010). The HIX values of >5 reflect the fresh OM derived from biomass and animal manure (Birdwell and Engel, 2010).

FI_{WSBrC} and $FI_{WI\text{-}MSBrC}$ ranged from 1.13 to 1.63, with averages of 1.38 and 1.29–2.24 (avg 1.60), respectively, during the campaign in Tianjin, while BIX_{WSBrC} and $BIX_{WI\text{-}MSBrC}$ were 0.79–1.39 (1.05) and 0.83–1.76 (1.26), respectively, during the campaign. Both the FI and BIX of WSBrC and WI-MSBrC followed a temporal pattern, but the temporal pattern of FI_{WSBrC} was exactly opposite to that of $FI_{WI\text{-}MSBrC}$ (Fig. 4a). The FI_{WSBrC} values slightly decreased from summer to fall, followed by a gradual increase to mid-winter and then a gradual decrease to summer through spring (Fig. 4a), while the temporal variations of BIX_{WSBrC} showed a gradual decrease from summer to fall followed by a gradual increase to winter and remained relatively stable during the winter, followed by a gradual decrease to summer through spring (Fig. 4b). The temporal variations of $BIX_{WI\text{-}MSBrC}$ were also found to be opposite to those of BIX_{WSBrC}, except in winter, in which the $BIX_{WI\text{-}MSBrC}$ values were higher compared to those in the other seasons (Fig. 4b). Interestingly, the temporal patterns of HIX_{WSBrC} and $HIX_{WI\text{-}MSBrC}$ were found to be similar: relatively stable in summer, followed by a sharp increase in early fall and then a gradual decrease to summer through winter and spring (Fig. 4c). Further, HIX_{WSBrC} was always significantly

higher than $HIX_{WI\text{-}MSBrC}$. Such temporal differences in all three fluorescence indices clearly indicate that the composition and/or aromaticity of WSBrC and WI-MSBrC are substantially distinct, even though they might have been mainly derived from similar sources: biomass burning and coal combustion, as discussed in the previous section.

The average FI_{WSBrC} was found to be higher in fall, followed by similar levels in winter and spring and the lowest ones in summer, whereas that of BIX_{WSBrC} was higher in winter, followed by fall, spring and summer (Table 1). The averages of both $FI_{WI\text{-}MSBrC}$ and $BIX_{WI\text{-}MSBrC}$ were higher in winter, followed by summer, spring and fall (Table 1). Annual and seasonal averages of FI values of both WSBrC and WI-MSBrC were around or higher than 1.4 and lower than 1.9 in Tianjin, indicating that the BrC in Tianjin was mainly derived from terrestrial OM that should have largely consisted of highly aromatic compounds. In contrast, the annual and seasonal averages of the BIX of both WSBrC and WI-MSBrC were higher than 1.0 (Table 1), indicating predominant contributions of OM from biological (including biomass burning) sources. In addition, the lowest FI_{WSBrC} and BIX_{WSBrC} values in summer and those of $FI_{WI\text{-}MSBrC}$ in spring and $BIX_{WI\text{-}MSBrC}$ in fall suggest that the contribution from terrestrial sources (e.g., coal combustion) might be less in spring and fall and that the photobleaching of OA might be significant under high solar radiation in summer.

HIX_{WSBrC} and $HIX_{WI\text{-}MSBrC}$ ranged from 1.72 to 4.7 with averages of 2.87 and 0.11–2.38 (avg 0.81), respectively, during the campaign, which again supports both the BrC components in Tianjin being significantly derived from biomass burning and consisting of highly humified and aromatic compounds. The average HIX_{WSBrC} was higher in summer, followed by fall, spring and winter (Table 1). In contrast, the average $HIX_{WI\text{-}MSBrC}$ was higher in winter, followed by fall, spring and summer (Table 1). It has been reported that aging processes and HIX have a significant relation (Deng et al., 2022). The higher HIX_{WSBrC} and lower $HIX_{WI\text{-}MSBrC}$ in summer confirm that the BrC, which is more water-soluble, was significantly produced from aromatic compounds and subject to significant atmospheric aging in summer over the Tianjin region.

3.3.2 Fluorophore identification

It is well established that fluorophores with different excitation emission wavelengths can distinguish between their types and sources. However, the types and sources of a large number of fluorophores have not been determined due to their complex chemical composition and sources. Here, we separated several fluorescence components from the EEM data using the PARAFAC model, and the results are shown in Fig. 5. The fact of the value of core consistency close to 100 in the PARAFAC model indicates that the more individual components that are analyzed together make up 100 % of the mixture, with no unexplained residues. The core consistency of the PARAFAC model explained the maximum variances of 89 % for WSBrC and 95 % for WI-MSBrC whole data obtained during the campaign, when three independent groups were chosen for the simulation.

The types of fluorophores of both WSBrC and WI-MSBrC identified in this study together with their excitation and emission wavelengths and those reported in the literature are summarized in Table 2. Among the total of three types of fluorophores obtained for WSBrC in Tianjin $PM_{2.5}$ by PARAFAC for EEMs, two showed fluorescence characteristics similar to those of less oxygenated and highly oxygenated HULIS, respectively, and the third one was similar to those of protein compounds (PLOM). Fluorophore $C1_{WSBrC}$ has a primary fluorescence peak at excitation/emission (Ex/Em), $< 240/393$ nm, and a secondary fluorescence peak at Ex/Em, 318/393 nm. $C1_{WSBrC}$ can be classified as a humus-like fluorophore because the bimodal distribution of the fluorescence spectrum is usually associated with HULIS. The emission wavelength of $C1_{WSBrC}$ was closer to the UV region than that of the second peak of $C2_{WSBrC}$, indicating the existence of a small number of aromatic substances, conjugate systems and nonlinear ring systems (Deng et al., 2022). $C2_{WSBrC}$ (Ex/Em $\sim$ 251, 363/462 nm) was identified as a common HULIS in aerosols, with higher oxidation, aromatization, molecular weight, conjugation and unsaturation due to its larger emission wavelength (Wen et al., 2021). The molecular weight of the fluorophore and its degree of conjugation tend to increase with the excitation wavelength, and such an increase in size and the conjugation degree may be attributed to the presence of highly aromatic conjugated structures containing heteroatoms (Chen et al., 2019). Compared to $C1_{WSBrC}$ and $C2_{WSBrC}$, $C3_{WSBrC}$ also contains two peaks, with a shorter-wavelength (< 380 nm) emission peak, which is usually associated with PLOM such as tryptophan and tyrosine, with low aromatic properties and small molecular sizes (Table 2).

However, WI-MSBrC fluorophore $C1_{WI\text{-}MSBrC}$ might be a tyrosine-like substance. $C2_{WI\text{-}MSBrC}$ is not quite certain and could be either HULIS or PLOM, because its emission wavelength of < 380 nm generally fits the profile of PLOM, but it is also close to the emission wavelength of HULIS, while $C3_{WI\text{-}MSBrC}$ is a tryptophan-like substance, which was reported to contain less aromatic and small molecular weight compounds. In general, phenols contribute significantly to $C3_{WI\text{-}MSBrC}$ fluorophores as they are the products of incomplete pyrolysis of lignin and cellulose and are used as indicators of biomass burning (Wen et al., 2021). Therefore, WI-MSBrC fluorophores of all samples in this study can be classified as mainly PLOM.

The percent contributions of each fluorophore to WSBrC and WI-MSBrC in $PM_{2.5}$ in Tianjin in each season are shown in Fig. 6. The compositions of WSBrC and WI-BrC clearly imply that the former contained more HULIS, whereas the latter consist mostly of PLOM and also indicate that most of

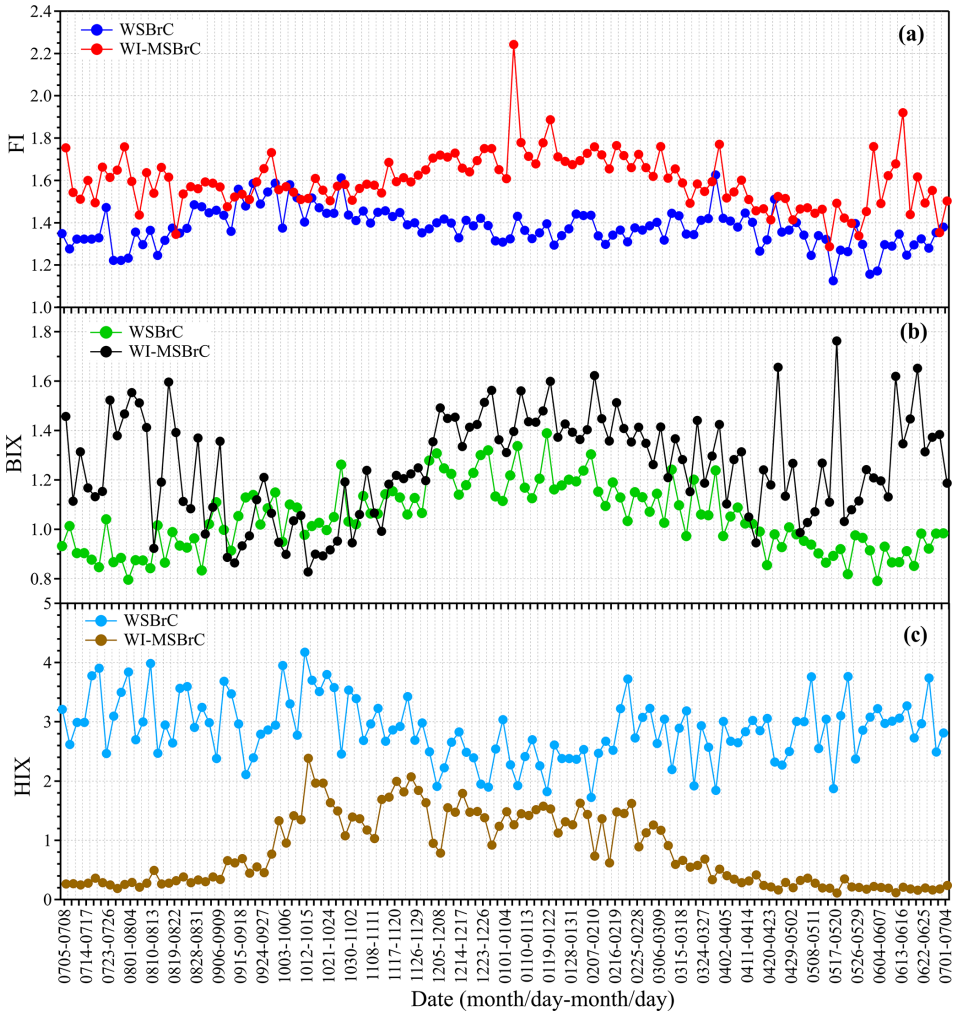

Figure 4. Temporal variations in light absorption and fluorescence properties of BrC in $PM_{2.5}$ in Tianjin: **(a)** FI, **(b)** BIX and **(c)** HIX.

the fluorophores of protein-like substances could dissolve in organic solvent rather than in water.

According to the excitation emission wavelength, we classified the fluorescence component of WI-MSBrC substances as PLOM, but the correlation between their fluorescence intensity and BIX ($R = 0.66$, $p < 0.05$) was very small, far lower than that of the WSBrC substance and BIX ($R = 0.59$, $p < 0.05$). By contrast, the correlation between their fluorescence intensity and HIX ($R = 0.74$, $p < 0.05$) was much higher than that of WSBrC ($R = -0.10$, $p < 0.05$). Although PLOM may be associated with some polycyclic aromatic hydrocarbons (PAHs) or phenols from fossil-fuel combustion and biomass burning, especially in urban aerosols, the correlation is puzzling.

On average, the humic-like fluorophores together contributed more than 60 % to the fluorescence intensity in WSBrC, suggesting that humic-like fluorophores played a dominant role in fluorescence properties of WSBrC in Tianjin. Generally, the low-oxygenated fluorophores $C1_{WSBrC}$ made considerable contributions in each season, while $C2_{WSBrC}$ highly oxygenated HULIS has a greater relative contribution in summer, which might be due to the strong solar radiation in summer. In contrast, in WI-MSBrC, the average contribution of PLOM to fluorescence intensity was higher than 70 % in spring (80.2 %) and summer (77.9 %), but the $C2_{WI\text{-}MSBrC}$ component dominated in winter and fall. This indicated that biological activities increased in spring and summer, and the relative abundance of bioaerosols might be higher during that period.

3.4 Potential sources of BrC

To further explore the potential sources of BrC, correlations of FV with chemical components and light absorption of $PM_{2.5}$ were examined. The sum of FVs of WSBrC and WI-MSBrC ($FVs_{(WSBrC+WI\text{-}MSBrC)}$) showed a significant correlation with secondary OC (SOC) in fall ($R = 0.90$, $p < 0.05$) and winter ($R = 0.67$, $p < 0.05$). Furthermore, the correla-

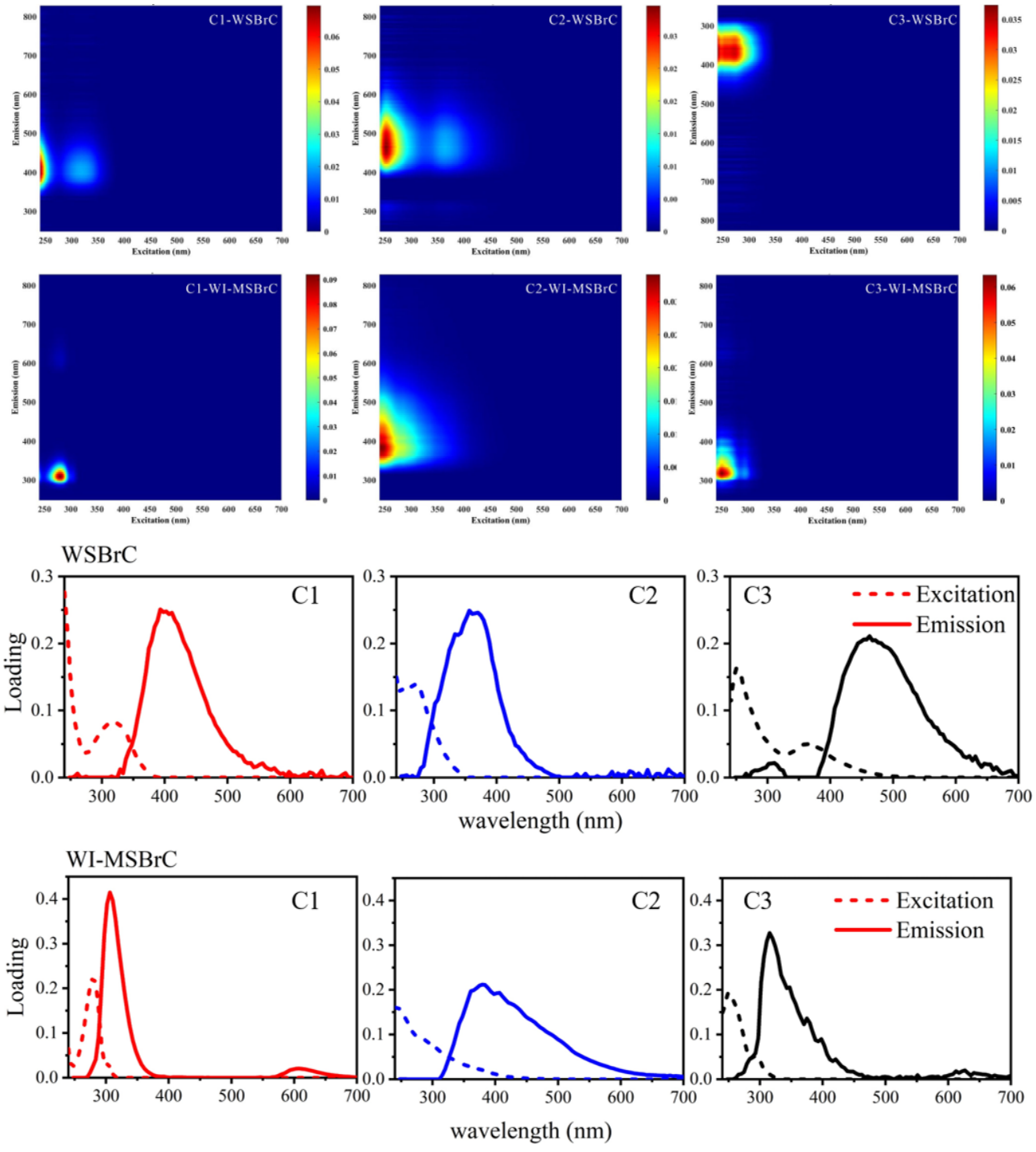

Figure 5. Three-dimensional excitation emission matrix of three fluorescent components (upper panel) together with their excitation and emission loadings (lower panel) of WSBrC and WI-MSBrC obtained by PARAFAC model analysis.

tion between $FVs_{(WSBrC+WI\text{-}MSBrC)}$ and EC in each season was insignificant. Such relations suggest that the secondary formation processes should have played an important role in controlling the loadings of BrC in fall and winter as well. A good correlation between the FV and Abs_{365} of both WSBrC and WI-MSBrC was found in all the seasons except winter, which indicates that most light-absorbing materials would also have significant fluorescence characteristics.

The relative contents of different chromophores in different polar extracts depend on their sources and varied signif-

Table 2. Description and wavelength positions of PARAFAC components in this study and other reports from the literature. (PLOM: protein compounds; HULIS: humic-like substances.)

Category	Components	Ex (nm)	Em (nm)	Substances	References
WSBrC	C1	< 240, 318	393	Low-oxygenated HULIS	This study
	C2	251, 363	462	Highly oxygenated HULIS	
	C3	< 240, 271	356.3	PLOM, such as tryptophan and tyrosine	
WI-MSBrC	C1	< 240, 279	306	PLOM, tyrosine-like	
	C2	< 240	379	Uncertain	
	C3	251, 294	315	PLOM, tryptophan-like	
Water-soluble BrC	C1	250, 315	396	Low-oxygenated HULIS	Deng et al. (2022)
	C2	250	465	Highly oxygenated HULIS	
	C3	250	385	Low-oxygenated HULIS	
	C4	250	340	PLOM, tryptophan-like	
	C5	275	305	PLOM, tyrosine-like	
WSOC	C1	240, 315	393	Low-oxygenated HULIS	Wen et al. (2021)
	C2	245, 360	476	Highly oxygenated HULIS	
	C3	< 240, 290	361	PLOM, such as tryptophan and tyrosine	
	C4	275	311	PLOM, tyrosine-like	
WSM and MSM	C1	255	415	HULIS-1 component	Chen et al. (2019)
	C2	220	340	Tryptophan-like component	
	C3	255	385	HULIS-2 component	
	C4	210	300	Tyrosine-like component	
	C5	250	355	Amino-acid-like component	
WSOC	C1	245	410	HULIS, photodegradation of macromolecules	Xie et al. (2020)
	C2	235	398	HULIS, aromatic and saturated compounds presented	
	C3	250, 360	466	Humic-like chromophores, more aromatic and consisting of more unsaturated compounds produced by condensation reactions	
	C4	250, 285	432	Terrestrial humic-like chromophore	
MSOC	C5	< 235	430	Terrestrial humic-like substance, photochemical product	
	C6	275	408	Low-oxygenated, humic-like	
	C7	235, 275	372	Protein-like chromophore	
	C8	260, 310	364	Protein-like (tryptophan-like), possibly related to PAHs	

icantly. The results showed that the NFVs of WSBrC were lower than those of WI-MSBrC and were different from season to season in Tianjin (Fig. 7). Recently, it was reported that the aerosols derived from biomass burning and coal combustion exhibit the highest NFV values, while SOA shows the lowest NFV values (Chen et al., 2020). NFVs in all the samples studied in Tianjin during 2018–2019 were very similar to those of primary emissions and higher than those of secondary aerosols. Such results reveal that the fluorophores in the Tianjin $PM_{2.5}$ might mainly be derived from primary combustion sources as well. In addition, the NFVs of the Tianjin $PM_{2.5}$ were higher in winter than in summer, which is likely and can be attributed to the photolysis of chromophores in summer. In addition, NFVs of WI-MSBrC were much higher than those of WSBrC, which indicates that the fluorescence contribution of fluorophores was more abundant in WI-MSBrC than in WSBrC.

4 Summary and conclusions

This study presents the temporal variations in light absorption and fluorescence properties of water-soluble BrC (WSBrC) and water-insoluble but MeOH-soluble BrC (WI-MSBrC) in $PM_{2.5}$ collected from Tianjin, North China, during 5 July 2018–4 July 2019. Light absorption properties of WSBrC and WI-MSBrC in Tianjin were investigated and found to be distinct from season to season, which was lower in spring and summer compared with that in fall and winter. The AAE of WI-MSBrC was comparable with that of WSBrC. The mass absorption efficiency of WSBrC and WI-MSBrC (MAE_{365}) exhibited distinct seasonal variations,

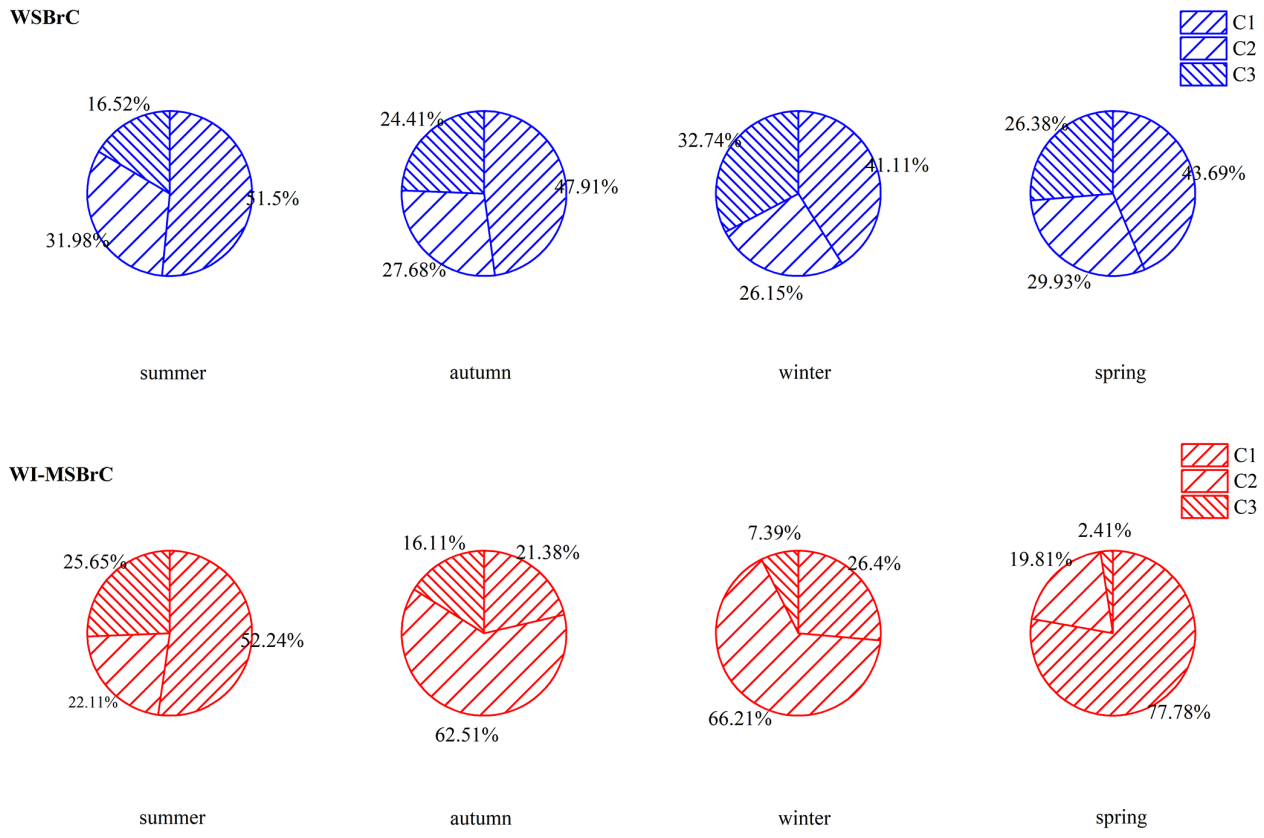

Figure 6. Relative abundances of the chromophores of the WSBrC and WI-MSBrC in $PM_{2.5}$ from Tianjin.

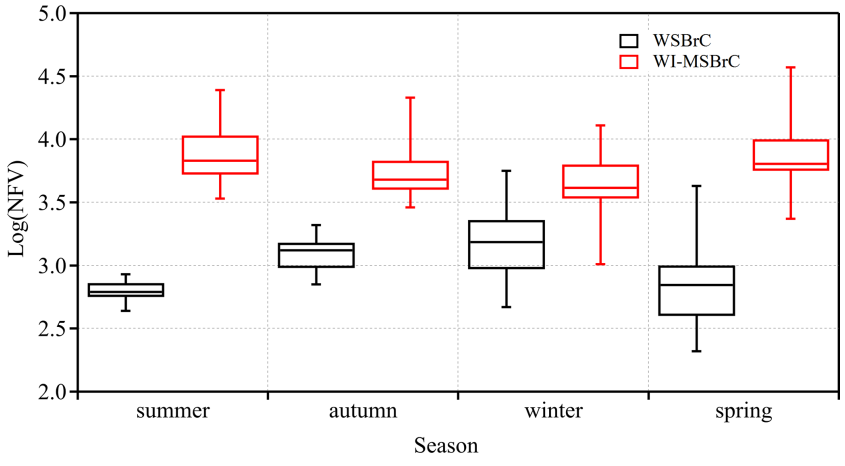

Figure 7. The normalized fluorescence volumes (NFVs) of the WSBrC and WI-MSBrC of $PM_{2.5}$ from Tianjin, North China.

which was higher in winter and lower in summer and fall. Biologically derived or secondary BrC and/or its photobleaching might be the reasons for the lower MAE_{365} values in summer and fall. The light absorption of both WSBrC and WI-MSBrC in the range of 300–400 nm to that in the whole range (300–700 nm) was ~40 %, indicating that BrC in the UV–Vis range plays an important role in climate warming. In addition, based on the PARAFAC analysis model, EEM data were comprehensively analyzed to identify the types and abundance of different fluorophores and obtained three types of fluorophores: low-oxygenated HULIS, highly oxygenated HULIS and protein-like compounds (PLOM). The correlation between BrC optical properties and aerosol chemical composition indicated that biomass burning and fossil-fuel (mainly coal) combustion significantly contributed to BrC content in winter, while primary biological emission and sub-

sequent aging significantly contributed to the BrC content in summer. These results illustrated the light absorption properties of BrC in metropolis aerosols and emphasized its significant contribution to radiative forcing.

Data availability. The data used in this study can be found online at https://doi.org/10.5281/zenodo.7316371 (Dong et al., 2022) and at https://doi.org/10.5281/zenodo.5140861 (Dong et al., 2021).

Supplement. The supplement related to this article is available online at: https://doi.org/10.5194/acp-24-5887-2024-supplement.

Author contributions. ZD and CMP conceptualized this study. ZD and PL conducted the sampling. ZD conducted the chemical analyses, interpreted the data, and wrote the manuscript. CMP supervised the research and acquired the funding for this study. ZX, XuZ and XiZ administrated the project. CMP, ZX, JD, PF and CQL contributed by discussing the results and reviewing and editing the manuscript.

Competing interests. The contact author has declared that none of the authors has any competing interests.

Disclaimer. Publisher's note: Copernicus Publications remains neutral with regard to jurisdictional claims made in the text, published maps, institutional affiliations, or any other geographical representation in this paper. While Copernicus Publications makes every effort to include appropriate place names, the final responsibility lies with the authors.

Acknowledgements. We thank Yunting Xiao for his help in writing a code to calculate the SFE.

We are grateful to the reviewers and the editor for their constructive comments that significantly improved the quality of this paper.

Financial support. This research has been supported by the National Natural Science Foundation of China (grant nos. 41775120 and 42277090) and the National Key Research and Development Program of China (grant no. 2017YFC0212700).

Review statement. This paper was edited by James Allan and reviewed by Luis Miguel Feijo Barreira and two anonymous referees.

References

Andreae, M. O. and Gelencsér, A.: Black carbon or brown carbon? The nature of light-absorbing carbonaceous aerosols, Atmos. Chem. Phys., 6, 3131–3148, https://doi.org/10.5194/acp-6-3131-2006, 2006.

Baduel, C., Voisin, D., and Jaffrezo, J. L.: Comparison of analytical methods for Humic Like Substances (HULIS) measurements in atmospheric particles, Atmos. Chem. Phys., 9, 5949–5962, https://doi.org/10.5194/acp-9-5949-2009, 2009.

Battin, T. J.: Dissolved organic matter and its optical properties in a blackwater tributary of the upper Orinoco river, Venezuela, Org. Geochem., 28, 561–569, https://doi.org/10.1016/S0146-6380(98)00028-X, 1998.

Birdwell, J. E. and Engel, A. S.: Characterization of dissolved organic matter in cave and spring waters using UV-Vis absorbance and fluorescence spectroscopy, Org. Geochem., 41, 270–280, https://doi.org/10.1016/j.orggeochem.2009.11.002, 2010.

Bond, T. C. and Bergstrom, R. W.: Light absorption by carbonaceous particles: An investigative review, Aerosol Sci. Tech., 40, 27–67, https://doi.org/10.1080/02786820500421521, 2006.

Brown, H., Liu, X., Pokhrel, R., Murphy, S., Lu, Z., Saleh, R., Mielonen, T., Kokkola, H., Bergman, T., Myhre, G., Skeie, R. B., Watson-Paris, D., Stier, P., Johnson, B., Bellouin, N., Schulz, M., Vakkari, V., Beukes, J. P., van Zyl, P. G., Liu, S., and Chand, D.: Biomass burning aerosols in most climate models are too absorbing, Nat. Commun., 12, 277, https://doi.org/10.1038/s41467-020-20482-9, 2021.

Cao, T., Li, M., Xu, C., Song, J., Fan, X., Li, J., Jia, W., and Peng, P.: Technical note: Chemical composition and source identification of fluorescent components in atmospheric water-soluble brown carbon by excitation–emission matrix spectroscopy with parallel factor analysis – potential limitations and applications, Atmos. Chem. Phys., 23, 2613–2625, https://doi.org/10.5194/acp-23-2613-2023, 2023.

Chen, Q., Fumikazu, I., Hayato, H., Daichi, A., and Michihiro, M.: Chemical structural characteristics of HULIS and other fractionated organic matter in urban aerosols: Results from mass spectral and FT-IR analysis, Environ. Sci. Technol., 50, 1721–1730, https://doi.org/10.1021/acs.est.5b05277, 2016a.

Chen, Q., Miyazaki, Y., Kawamura, K., Matsumoto, K., Coburn, S., Volkamer, R., Iwamoto, Y., Kagami, S., Deng, Y., Ogawa, S., Ramasamy, S., Kato, S., Ida, A., Kajii, Y., and Mochida, M.: Characterization of chromophoric water-soluble organic matter in urban, forest, and marine aerosols by HR-ToF-AMS analysis and excitation–emission matrix spectroscopy, Environ. Sci. Technol., 50, 10351–10360, https://doi.org/10.1021/acs.est.6b01643, 2016b.

Chen, Q., Mu, Z., Song, W., Wang, Y., Yang, Z., Zhang, L., and Zhang, Y.-L.: Size-resolved characterization of the chromophores in atmospheric particulate matter from a typical coal-burning city in China, J. Geophys. Res.-Atmos., 124, 10546–10563, https://doi.org/10.1029/2019JD031149, 2019.

Chen, Q., Li, J., Hua, X., Jiang, X., Mu, Z., Wang, M., Wang, J., Shan, M., Yang, X., Fan, X., Song, J., Wang, Y., Guan, D., and Du, L.: Identification of species and sources of atmospheric chromophores by fluorescence excitation-emission matrix with parallel factor analysis, Sci. Total Environ., 718, 137322, https://doi.org/10.1016/j.scitotenv.2020.137322, 2020.

Chen, Q. C., Ikemori, F., and Mochida, M.: Light Absorption and Excitation-Emission Fluorescence of Urban Organic Aerosol Components and Their Relationship to Chemical Structure, Environ. Sci. Technol., 50, 10859–10868, https://doi.org/10.1021/acs.est.6b02541, 2016.

Choudhary, V., Rajput, P., and Gupta, T.: Absorption properties and forcing efficiency of light-absorbing water-soluble organic aerosols: Seasonal and spatial variability, Environ. Pollut., 272, 115932, https://doi.org/10.1016/j.envpol.2020.115932, 2021.

Coble, P. G.: Marine optical biogeochemistry: The chemistry of ocean color, Chem. Rev., 107, 402–418, https://doi.org/10.1021/cr050350+, 2007.

Corbin, J. C., Czech, H., Massabò, D., de Mongeot, F. B., Jakobi, G., Liu, F., Lobo, P., Mennucci, C., Mensah, A. A., Orasche, J., Pieber, S. M., Prévôt, A. S. H., Stengel, B., Tay, L. L., Zanatta, M., Zimmermann, R., El Haddad, I., and Gysel, M.: Infrared-absorbing carbonaceous tar can dominate light absorption by marine-engine exhaust, npj Climate and Atmospheric Science, 2, 12, https://doi.org/10.1038/s41612-019-0069-5, 2019.

Deng, J., Ma, H., Wang, X., Zhong, S., Zhang, Z., Zhu, J., Fan, Y., Hu, W., Wu, L., Li, X., Ren, L., Pavuluri, C. M., Pan, X., Sun, Y., Wang, Z., Kawamura, K., and Fu, P.: Measurement report: Optical properties and sources of water-soluble brown carbon in Tianjin, North China – insights from organic molecular compositions, Atmos. Chem. Phys., 22, 6449–6470, https://doi.org/10.5194/acp-22-6449-2022, 2022.

Diggs, D. L., Huderson, A. C., Harris, K. L., Myers, J. N., Banks, L. D., Rekhadevi, P. V., Niaz, M. S., and Ramesh, A.: Polycyclic aromatic hydrocarbons and digestive tract cancers: a perspective, J. Environ. Sci. Heal. C, 29, 324–357, https://doi.org/10.1080/10590501.2011.629974, 2011.

Dong, Z., Pavuluri, C. M., Xu, Z., Wang, Y., Li, P., Fu, P., and Liu, C.-Q.: Year-round observations of bulk components and 13C and 15N isotope ratios of fine aerosols at Tianjin, North China, Zenodo [data set], https://doi.org/10.5281/zenodo.5140861, 2021.

Dong, Z., Pavuluri, C. M., Li, P., Xu, Z., Deng, J., Zhao, X., and Zhao, X.: Year-round observations of the optical properties of brown carbon in fine aerosols at Tianjin, North China, Zenodo [data set], https://doi.org/10.5281/zenodo.7316371, 2022.

Dong, Z., Pavuluri, C. M., Xu, Z., Wang, Y., Li, P., Fu, P., and Liu, C.-Q.: Measurement report: Chemical components and ^{13}C and ^{15}N isotope ratios of fine aerosols over Tianjin, North China: year-round observations, Atmos. Chem. Phys., 23, 2119–2143, https://doi.org/10.5194/acp-23-2119-2023, 2023.

Fan, X., Wei, S., Zhu, M., Song, J., and Peng, P.: Comprehensive characterization of humic-like substances in smoke $PM_{2.5}$ emitted from the combustion of biomass materials and fossil fuels, Atmos. Chem. Phys., 16, 13321–13340, https://doi.org/10.5194/acp-16-13321-2016, 2016.

Feng, Y., Ramanathan, V., and Kotamarthi, V. R.: Brown carbon: a significant atmospheric absorber of solar radiation?, Atmos. Chem. Phys., 13, 8607–8621, https://doi.org/10.5194/acp-13-8607-2013, 2013.

Gao, Y. and Zhang, Y.: Formation and photochemical investigation of brown carbon by hydroxyacetone reactions with glycine and ammonium sulfate, Royal Society of Chemistry Advances, 8, 20719–20725, https://doi.org/10.1039/C8RA02019A, 2018.

Gu, Q. and Kenny, J. E.: Improvement of inner filter effect correction based on determination of effective geometric parameters using a conventional fluorimeter, Anal. Chem., 81, 420–426, https://doi.org/10.1021/ac801676j, 2009.

Hecobian, A., Zhang, X., Zheng, M., Frank, N., Edgerton, E. S., and Weber, R. J.: Water-Soluble Organic Aerosol material and the light-absorption characteristics of aqueous extracts measured over the Southeastern United States, Atmos. Chem. Phys., 10, 5965–5977, https://doi.org/10.5194/acp-10-5965-2010, 2010.

Hems, R. F., Schnitzler, E. G., Liu-Kang, C., Cappa, C. D., and Abbatt, J. P. D.: Aging of atmospheric brown carbon aerosol, ACS Earth and Space Chemistry, 5, 722–748, https://doi.org/10.1021/acsearthspacechem.0c00346, 2021.

Hoffer, A., Gelencsér, A., Guyon, P., Kiss, G., Schmid, O., Frank, G. P., Artaxo, P., and Andreae, M. O.: Optical properties of humic-like substances (HULIS) in biomass-burning aerosols, Atmos. Chem. Phys., 6, 3563–3570, https://doi.org/10.5194/acp-6-3563-2006, 2006.

Huang, R. J., Yang, L., Cao, J., Chen, Y., Chen, Q., Li, Y., Duan, J., Zhu, C., Dai, W., Wang, K., Lin, C., Ni, H., Corbin, J. C., Wu, Y., Zhang, R., Tie, X., Hoffmann, T., O'Dowd, C., and Dusek, U.: Brown carbon aerosol in urban Xi'an, Northwest China: The composition and light absorption properties, Environ. Sci. Technol., 52, 6825–6833, https://doi.org/10.1021/acs.est.8b02386, 2018.

Huang, R. J., Yang, L., Shen, J., Yuan, W., Gong, Y., Guo, J., Cao, W., Duan, J., Ni, H., Zhu, C., Dai, W., Li, Y., Chen, Y., Chen, Q., Wu, Y., Zhang, R., Dusek, U., O'Dowd, C., and Hoffmann, T.: Water-insoluble organics dominate brown carbon in wintertime urban aerosol of China: Chemical characteristics and optical properties, Environ. Sci. Technol., 54, 7836–7847, https://doi.org/10.1021/acs.est.0c01149, 2020.

Jo, D. S., Park, R. J., Lee, S., Kim, S.-W., and Zhang, X.: A global simulation of brown carbon: implications for photochemistry and direct radiative effect, Atmos. Chem. Phys., 16, 3413–3432, https://doi.org/10.5194/acp-16-3413-2016, 2016.

Kasthuriarachchi, N. Y., Rivellini, L.-H., Chen, X., Li, Y. J., and Lee, A. K. Y.: Effect of relative humidity on secondary brown carbon formation in aqueous droplets, Environ. Sci. Technol., 54, 13207–13216, https://doi.org/10.1021/acs.est.0c01239, 2020.

Lack, D. A., Bahreini, R., Langridge, J. M., Gilman, J. B., and Middlebrook, A. M.: Brown carbon absorption linked to organic mass tracers in biomass burning particles, Atmos. Chem. Phys., 13, 2415–2422, https://doi.org/10.5194/acp-13-2415-2013, 2013.

Laskin, A., Laskin, J., and Nizkorodov, S. A.: Chemistry of Atmospheric Brown Carbon, Chem. Rev., 115, 4335–4382, https://doi.org/10.1021/cr5006167, 2015.

Lawaetz, A. J. and Stedmon, C. A.: Fluorescence intensity calibration using the Raman scatter peak of water, Appl. Spectrosc., 63, 936–940, https://doi.org/10.1366/000370209788964548, 2009.

Lee, H. J., Laskin, A., Laskin, J., and Nizkorodov, S. A.: Excitation-Emission Spectra and Fluorescence Quantum Yields for Fresh and Aged Biogenic Secondary Organic Aerosols, Environ. Sci. Technol., 47, 5763–5770, https://doi.org/10.1021/es400644c, 2013.

Lesworth, T., Baker, A. R., and Jickells, T.: Aerosol organic nitrogen over the remote Atlantic Ocean, Atmos. Environ., 44, 1887–1893, https://doi.org/10.1016/j.atmosenv.2010.02.021, 2010.

Li, C., He, Q., Hettiyadura, A. P. S., Käfer, U., Shmul, G., Meidan, D., Zimmermann, R., Brown, S. S., George, C.,

Laskin, A., and Rudich, Y.: Formation of secondary brown carbon in biomass burning aerosol proxies through NO_3 radical reactions, Environ. Sci. Technol., 54, 1395–1405, https://doi.org/10.1021/acs.est.9b05641, 2020.

Li, J., Zhang, Q., Wang, G., Li, J., Wu, C., Liu, L., Wang, J., Jiang, W., Li, L., Ho, K. F., and Cao, J.: Optical properties and molecular compositions of water-soluble and water-insoluble brown carbon (BrC) aerosols in northwest China, Atmos. Chem. Phys., 20, 4889–4904, https://doi.org/10.5194/acp-20-4889-2020, 2020.

Li, S., Zhu, M., Yang, W. Q., Tang, M. J., Huang, X. L., Yu, Y. G., Fang, H., Yu, X., Yu, Q. Q., Fu, X. X., Song, W., Zhang, Y. L., Bi, X. H., and Wang, X. M.: Filter-based measurement of light absorption by brown carbon in $PM_{2.5}$ in a megacity in South China, Sci. Total Environ., 633, 1360–1369, https://doi.org/10.1016/j.scitotenv.2018.03.235, 2018.

Li, X., Fu, P., Tripathee, L., Yan, F., Hu, Z., Yu, F., Chen, Q., Li, J., Chen, Q., Cao, J., and Kang, S.: Molecular compositions, optical properties, and implications of dissolved brown carbon in snow/ice on the Tibetan Plateau glaciers, Environ. Int., 164, 107276, https://doi.org/10.1016/j.envint.2022.107276, 2022.

Liakakou, E., Kaskaoutis, D. G., Grivas, G., Stavroulas, I., Tsagkaraki, M., Paraskevopoulou, D., Bougiatioti, A., Dumka, U. C., Gerasopoulos, E., and Mihalopoulos, N.: Long-term brown carbon spectral characteristics in a Mediterranean city (Athens), Sci. Total Environ., 708, 135019, https://doi.org/10.1016/j.scitotenv.2019.135019, 2020.

Lin, G., Penner, J. E., Flanner, M. G., Sillman, S., Xu, L., and Zhou, C.: Radiative forcing of organic aerosol in the atmosphere and on snow: Effects of SOA and brown carbon, J. Geophys. Res.-Atmos., 119, 7453–7476, https://doi.org/10.1002/2013jd021186, 2014.

Lin, P., Bluvshtein, N., Rudich, Y., Nizkorodov, S. A., Laskin, J., and Laskin, A.: Molecular Chemistry of Atmospheric Brown Carbon Inferred from a Nationwide Biomass Burning Event, Environ. Sci. Technol., 51, 11561–11570, https://doi.org/10.1021/acs.est.7b02276, 2017.

Liu, J., Bergin, M., Guo, H., King, L., Kotra, N., Edgerton, E., and Weber, R. J.: Size-resolved measurements of brown carbon in water and methanol extracts and estimates of their contribution to ambient fine-particle light absorption, Atmos. Chem. Phys., 13, 12389–12404, https://doi.org/10.5194/acp-13-12389-2013, 2013.

McKnight, D. M., Boyer, E. W., Westerhoff, P. K., Doran, P. T., Kulbe, T., and Andersen, D. T.: Spectrofluorometric characterization of dissolved organic matter for indication of precursor organic material and aromaticity, Limnol. Oceanogr., 46, 38–48, https://doi.org/10.4319/lo.2001.46.1.0038, 2001.

Murphy, K. R., Stedmon, C. A., Graeber, D., and Bro, R.: Fluorescence spectroscopy and multi-way techniques. PARAFAC, Anal. Methods-UK, 5, 6557–6566, https://doi.org/10.1039/C3AY41160E, 2013.

Park, R. J., Kim, M. J., Jeong, J. I., Youn, D., and Kim, S.: A contribution of brown carbon aerosol to the aerosol light absorption and its radiative forcing in East Asia, Atmos. Environ., 44, 1414–1421, https://doi.org/10.1016/j.atmosenv.2010.01.042, 2010.

Peters, S., Talaska, G., Jonsson, B. A., Kromhout, H., and Vermeulen, R.: Polycyclic aromatic hydrocarbon exposure, urinary mutagenicity, and DNA adducts in rubber manufacturing workers, Cancer Epidem. Biomar., 17, 1452–1459, https://doi.org/10.1158/1055-9965.EPI-07-2777, 2008.

Qin, J., Zhang, L., Zhou, X., Duan, J., Mu, S., Xiao, K., Hu, J., and Tan, J.: Fluorescence fingerprinting properties for exploring water-soluble organic compounds in $PM_{2.5}$ in an industrial city of northwest China, Atmos. Environ., 184, 203–211, https://doi.org/10.1016/j.atmosenv.2018.04.049, 2018.

Rizzo, L. V., Correia, A. L., Artaxo, P., Procópio, A. S., and Andreae, M. O.: Spectral dependence of aerosol light absorption over the Amazon Basin, Atmos. Chem. Phys., 11, 8899–8912, https://doi.org/10.5194/acp-11-8899-2011, 2011.

Rizzo, L. V., Artaxo, P., Müller, T., Wiedensohler, A., Paixão, M., Cirino, G. G., Arana, A., Swietlicki, E., Roldin, P., Fors, E. O., Wiedemann, K. T., Leal, L. S. M., and Kulmala, M.: Long term measurements of aerosol optical properties at a primary forest site in Amazonia, Atmos. Chem. Phys., 13, 2391–2413, https://doi.org/10.5194/acp-13-2391-2013, 2013.

Saleh, R.: From Measurements to Models: Toward Accurate Representation of Brown Carbon in Climate Calculations, Current Pollution Reports, 6, 90–104, https://doi.org/10.1007/s40726-020-00139-3, 2020.

Shamjad, P. M., Tripathi, S. N., Thamban, N. M., and Vreeland, H.: Refractive Index and Absorption Attribution of Highly Absorbing Brown Carbon Aerosols from an Urban Indian City-Kanpur, Sci. Rep.-UK, 6, 37735, https://doi.org/10.1038/srep37735, 2016.

Shetty, N. J., Pandey, A., Baker, S., Hao, W. M., and Chakrabarty, R. K.: Measuring light absorption by freshly emitted organic aerosols: optical artifacts in traditional solvent-extraction-based methods, Atmos. Chem. Phys., 19, 8817–8830, https://doi.org/10.5194/acp-19-8817-2019, 2019.

Sun, J., Zhi, G., Hitzenberger, R., Chen, Y., Tian, C., Zhang, Y., Feng, Y., Cheng, M., Zhang, Y., Cai, J., Chen, F., Qiu, Y., Jiang, Z., Li, J., Zhang, G., and Mo, Y.: Emission factors and light absorption properties of brown carbon from household coal combustion in China, Atmos. Chem. Phys., 17, 4769–4780, https://doi.org/10.5194/acp-17-4769-2017, 2017.

Tang, J., Li, J., Mo, Y., Safaei Khorram, M., Chen, Y., Tang, J., Zhang, Y., Song, J., and Zhang, G.: Light absorption and emissions inventory of humic-like substances from simulated rainforest biomass burning in Southeast Asia, Environ. Pollut., 262, 114266, https://doi.org/10.1016/j.envpol.2020.114266, 2020.

Wang, D., Shen, Z., Zhang, Q., Lei, Y., Zhang, T., Huang, S., Sun, J., Xu, H., and Cao, J.: Winter brown carbon over six of China's megacities: light absorption, molecular characterization, and improved source apportionment revealed by multilayer perceptron neural network, Atmos. Chem. Phys., 22, 14893–14904, https://doi.org/10.5194/acp-22-14893-2022, 2022.

Wang, Q. Q., Zhou, Y. Y., Ma, N., Zhu, Y., Zhao, X. C., Zhu, S. W., Tao, J. C., Hong, J., Wu, W. J., Cheng, Y. F., and Su, H.: Review of brown carbon aerosols in China: Pollution level, optical properties, and emissions, J. Geophys. Res.-Atmos., 127, e2021JD035473, https://doi.org/10.1029/2021JD035473, 2022.

Wang, Y., Pavuluri, C. M., Fu, P., Li, P., Dong, Z., Xu, Z., Ren, H., Fan, Y., Li, L., Zhang, Y.-L., and Liu, C.-Q.: Characterization of Secondary Organic Aerosol Tracers over Tianjin, North China during Summer to Autumn, ACS Earth and Space Chemistry, 3, 2339–2352, https://doi.org/10.1021/acsearthspacechem.9b00170, 2019.

Wen, H., Zhou, Y., Xu, X., Wang, T., Chen, Q., Chen, Q., Li, W., Wang, Z., Huang, Z., Zhou, T., Shi, J., Bi, J., Ji, M., and Wang, X.: Water-soluble brown carbon in atmospheric aerosols along the transport pathway of Asian dust: Optical properties, chemical compositions, and potential sources, Sci. Total Environ., 789, 147971, https://doi.org/10.1016/j.scitotenv.2021.147971, 2021.

Wu, G. M., Fu, P. Q., Ram, K., Song, J. Z., Chen, Q. C., Kawamura, K., Wan, X., Kang, S. C., Wang, X. P., Laskin, A., and Cong, Z. Y.: Fluorescence characteristics of water-soluble organic carbon in atmospheric aerosol, Environ. Pollut., 268, 115906, https://doi.org/10.1016/j.envpol.2020.115906, 2021.

Xie, X., Chen, Y., Nie, D., Liu, Y., Liu, Y., Lei, R., Zhao, X., Li, H., and Ge, X.: Light-absorbing and fluorescent properties of atmospheric brown carbon: A case study in Nanjing, China, Chemosphere, 251, 126350, https://doi.org/10.1016/j.chemosphere.2020.126350, 2020.

Yan, J., Wang, X., Gong, P., Wang, C., and Cong, Z.: Review of brown carbon aerosols: Recent progress and perspectives, Sci. Total Environ., 634, 1475–1485, https://doi.org/10.1016/j.scitotenv.2018.04.083, 2018.

Yu, H., Liang, H., Qu, F., Han, Z. S., Shao, S., Chang, H., and Li, G.: Impact of dataset diversity on accuracy and sensitivity of parallel factor analysis model of dissolved organic matter fluorescence excitation-emission matrix, Sci. Rep.-UK, 5, 10207, https://doi.org/10.1038/srep10207, 2015.

Yue, S., Zhu, J., Chen, S., Xie, Q., Li, W., Li, L., Ren, H., Sihui, S., Ping, L., Ma, H., Fan, Y., Cheng, B., Wu, L., Deng, J., Hu, W., Ren, L., Lianfang, W., Zhao, W., Tian, Y., and Fu, P.: Brown carbon from biomass burning imposes strong circum-Arctic warming, One Earth, 5, 293–304, https://doi.org/10.1016/j.oneear.2022.02.006, 2022.

Yue, S. Y., Bikkina, S., Gao, M., Barrie, L., Kawamura, K., and Fu, P. Q.: Sources and Radiative Absorption of Water-Soluble Brown Carbon in the High Arctic Atmosphere, Geophys. Res. Lett., 46, 14881–14891, https://doi.org/10.1029/2019gl085318, 2019.

Zhan, Y., Li, J., Tsona, N. T., Chen, B., Yan, C., George, C., and Du, L.: Seasonal variation of water-soluble brown carbon in Qingdao, China: Impacts from marine and terrestrial emissions, Environ. Res., 212, 113144, https://doi.org/10.1016/j.envres.2022.113144, 2022.

Zhang, Q., Jimenez, J. L., Canagaratna, M. R., Ulbrich, I. M., Ng, N. L., Worsnop, D. R., and Sun, Y.: Understanding atmospheric organic aerosols via factor analysis of aerosol mass spectrometry: a review, Anal. Bioanal. Chem., 401, 3045–3067, https://doi.org/10.1007/s00216-011-5355-y, 2011.

Zhang, Q., Shen, Z., Zhang, T., Kong, S., Lei, Y., Wang, Q., Tao, J., Zhang, R., Wei, P., Wei, C., Cui, S., Cheng, T., Ho, S. S. H., Li, Z., Xu, H., and Cao, J.: Spatial distribution and sources of winter black carbon and brown carbon in six Chinese megacities, Sci. Total Environ., 762, 143075, https://doi.org/10.1016/j.scitotenv.2020.143075, 2021.

Zhong, M. and Jang, M.: Light absorption coefficient measurement of SOA using a UV–Visible spectrometer connected with an integrating sphere, Atmos. Environ., 45, 4263–4271, https://doi.org/10.1016/j.atmosenv.2011.04.082, 2011.

Zhu, C. S., Cao, J. J., Huang, R. J., Shen, Z. X., Wang, Q. Y., and Zhang, N. N.: Light absorption properties of brown carbon over the southeastern Tibetan Plateau, Sci. Total Environ., 625, 246–251, https://doi.org/10.1016/j.scitotenv.2017.12.183, 2018.